



City Research Online

City, University of London Institutional Repository

Citation: Boscolo, M. & Banerjee, J. R. (2014). Layer-wise dynamic stiffness solution for free vibration analysis of laminated composite plates. *Journal of Sound and Vibration*, 333(1), pp. 200-227. doi: 10.1016/j.jsv.2013.08.031

This is the accepted version of the paper.

This version of the publication may differ from the final published version.

Permanent repository link: <https://openaccess.city.ac.uk/id/eprint/14356/>

Link to published version: <https://doi.org/10.1016/j.jsv.2013.08.031>

Copyright: City Research Online aims to make research outputs of City, University of London available to a wider audience. Copyright and Moral Rights remain with the author(s) and/or copyright holders. URLs from City Research Online may be freely distributed and linked to.

Reuse: Copies of full items can be used for personal research or study, educational, or not-for-profit purposes without prior permission or charge. Provided that the authors, title and full bibliographic details are credited, a hyperlink and/or URL is given for the original metadata page and the content is not changed in any way.

City Research Online:

<http://openaccess.city.ac.uk/>

publications@city.ac.uk

Layer wise dynamic stiffness solution for free vibration analysis of laminated composite plates

M. Boscolo*, J. R. Banerjee

School of Engineering and Mathematical Sciences, City University London, Northampton Square, London, EC1V 0HB

Abstract

The dynamic stiffness method has been developed by using a sophisticated layer wise theory which complies with the C_z^0 requirements and delivers high accuracy for the analysis of laminated composite plates. The method is versatile as it derives the dynamic stiffness matrix for plates with any number of layers in a novel way without the need to re-derive and re-solve the equations of motion when the number of layers has changed. This novel procedure to manipulate and solve the equations of motion has been referred to as the L-matrix method in this paper. The Carrera unified formulation (CUF) is employed to derive the equations of motion of a plate through the use of a first order layer wise assumption for a plate with a single layer first. The method is then generalised and extended to multiple layers. Essentially by writing the equations of motion of one single layer in the L-matrix form, the system of equations of motion of a laminated plate with any number of layers is generated in an efficient and automatic way. A significant feature of the subsequent work is to devise a method to solve the system of differential

*Corresponding author

Email address: marco.boscolo.1@city.ac.uk (M. Boscolo)

equations automatically in closed analytical form and then obtain the ensuing dynamic stiffness matrix of the laminated plate. The developed dynamic stiffness element has been validated wherever possible by analytical solutions (based on Navier's solution for plates simply supported at all edges) for the same displacement formulation. Furthermore, the dynamic stiffness theory is assessed by 3D analytical solutions (scantly available in the literature) and also by the finite element method using NASTRAN. The results have been obtained in an exact sense for the first time and hence they can be used as benchmark solutions for assessing approximate methods. This new development of the dynamic stiffness method will allow free vibration and response analysis of geometrically complex structures with such a level of computational efficiency and accuracy that could not be possibly achieved using other methods.

Keywords: Dynamic stiffness method, benchmark solutions, Layer-wise theory, composites, free vibration analysis, Carrera Unified Formulation.

1. INTRODUCTION

Multilayered composite structures are increasingly being used in aircraft and other industries because of their high specific strengths and ability to be tailored for stiffness properties to satisfy specific design requirements. Over the past decades, the use of composite materials has been confined mostly to secondary (small or non-load carrying) structures such as aircraft ailerons, fins and rudders. The situation has changed in recent years and there have been significant inroads and progresses made in that composites have steadfastly made headways to primary structures. As a consequence, the develop-

ment of more advanced and accurate theories for modelling thick multilayered plates has been the focus of attention of many researchers during the past few years. A vast amount of literature is now available on the subject. The technique generally used to model a multilayered composite structure (constructed in the form of a laminate) is based on the classical lamination theory (CLT) [1]. This is a natural extension of the classical theory used for traditional single layer structure such as a plate. In CLT a multi-layered structure is thought to behave as a single layer having equivalent properties obtained by the superposition of all single layers. For this reason the theory is also called equivalent single layer (ESL) theory. Since a multi-layer structure is reduced to an equivalent single layer, classical plate theories, such as Kirchhoff classical plate theory (CPT), Reissner [2]-Mindlin [3] (first order shear deformation theory, FSDT) or higher order shear deformation theories (HSDT) [4], can be used to examine the static or dynamic behaviour. Although ESL theory based on either FSDT or HSDT has proved to be reasonably accurate to describe the macro behaviour of multilayered structures, it should be recognised that for thicker plates of in-plane dimension over thickness ratio ≤ 50 (often required in the design of primary structures), more advanced theories are needed to provide accurate results for the enhancement of existing design. One of the main problems of ESL theory is that C_z^0 requirements are not satisfied at the interface [5] which is a well known anomaly in the mechanics of laminated composites. The C_z^0 requirements have earlier been demonstrated by 3D exact solutions [6] and they can be summarised as follows:

- (i) Continuous displacements but discontinuous derivatives at the inter-

faces;

- (ii) Continuous normal and surface shear stresses ($\boldsymbol{\sigma}_n^T = \begin{bmatrix} \sigma_{zx}, \sigma_{zy}, \sigma_{zz} \end{bmatrix}$) at the interfaces.

It is clear that displacements must be continuous at the interfaces between layers if the interface has to remain intact. In the same way the normal stresses must be continuous to ensure equilibrium. In order to have continuous normal stresses and the continuity of displacements at the interface, the first derivative of displacements (strains) must be discontinuous since the material properties can be different from one layer to the other. This has meant that the in-plane stresses must be discontinuous without violating the equilibrium condition. Typical fields of stresses and displacements which comply with C_z^0 requirements are shown in Figure (1). In the ESL theory,

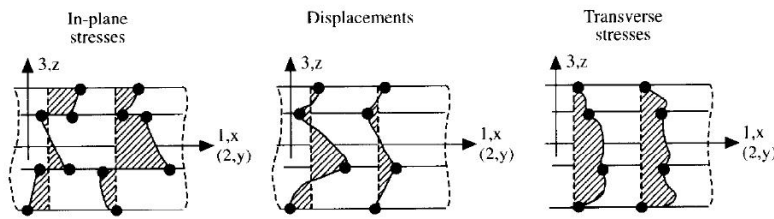


Figure 1: Example of real stress and displacement fields for multilayered structures [5]

an equivalent layer is studied and consequently, the displacements are considered continuous and differentiable through the interface, which no-doubt violates the C_z^0 requirements (Figure (2)). A method to overcome this problem is to add additional unknowns to model the zig-zag behaviour of the displacement field. These are referred to as zig-zag theories such as the ones published in [7–10] (Figure (2)). More accurate theories have been developed where each single layer is modelled as a plate and then connected through

thickness by using a suitable assembly procedure. This leads to the so-called layer-wise (LW) theory [5, 11–17]. Each single layer can be modelled using classical plate theory, FSDT or HSDT. The displacement functions are chosen appropriately so that the continuity of displacements can be imposed at the interfaces during the assembly procedure. The change in the slope at the interfaces is routinely obtained by solving the problem. The assumed displacement field through the thickness for an LW theory is illustrated in Figure (2). It is evident that if LW theory is used, the displacement field is more

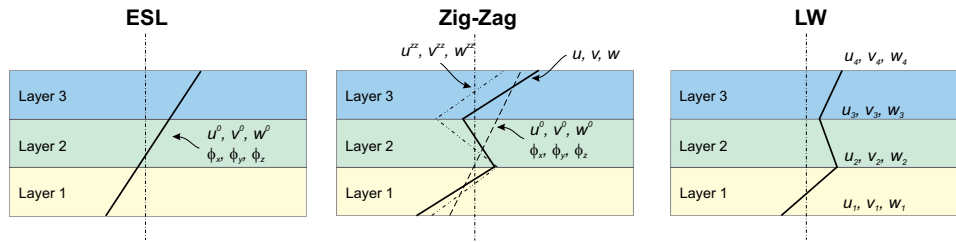


Figure 2: Example of first order ESL, Zig-Zag and LW displacement distributions through the thickness

accurately represented (see Figures (1) and (2)), and therefore, the results of the analysis will be more accurate. This is not only true for stress analysis, but also for displacement and modal analysis. The improvement in the accuracy of results will inevitably be significant for thick plates, particularly when the difference in properties from one layer to the other is considerable. A detailed review on the historical development of the above theories can be found in an exhaustive article published by Carrera [5] and also in [17–20] when dealing with the free vibration analysis of multilayered composite and sandwich plates. It was shown in these articles that the use of ESL theories could lead to large discrepancies when compared with the exact 3D results [6]

especially for large orthotropic and thickness ratios. Even for thin plates with typical width to thickness ratio of 50, the error on the fundamental frequency can be as high as 10% [18–20] or 30% for multifield problems [12], and completely wrong even by a order of magnitude for sandwich plates [17]. The need to use of a layer wise theory for obtaining accurate results cannot be overstated. Understandably the layer wise theory requires a large number of degrees of freedom which of course, depends on the number of layers. At present the problem is solved generally in exceptional circumstances by using the finite element method (FEM) [21] requiring a huge number of elements, thus embarking on an excessively large number of nodes to model the structure. This is probably the main reason why the layer wise theory is not favoured and often overlooked and, as an alternative, less accurate zig-zag theories are sought instead. Apparently the layer wise based finite elements are mainly (if not solely) used for modelling delamination in ABAQUS software (called continuous shell elements) requiring large computational resources.

Against this background, a first order layer wise theory based on the Carrera’s Unified Formulation (CUF) [12, 14, 16–20, 22, 23] is proposed in this paper. Instead of using the finite element solution, which requires exorbitantly large number of nodes, or a restricted analytical Navier type solution that is suitable only for a rectangular plate with all four sides simply supported, the Dynamic Stiffness Method (DSM) because of its elegant application and powerful modelling capability is considered here to be the best way forward. [24–46]. The DSM requires the closed form analytical solution of the free vibration problem of the structural element, and then, by applying

general boundary conditions, a dynamic stiffness matrix which contains all the natural frequencies of the element can be developed. This element for a plate has the shape of a strip that can be rotated and assembled to form a geometrically complex structure and yet the exactness of the solution can be retained. The results, in fact, will be mesh independent and with very few elements any number of required natural frequencies and mode shapes can be obtained to any desired accuracy for a structure that can be modelled or idealised as plate assemblies. The use of the DSM will allow an efficient use of LW theories because of the limited number of degrees of freedom required by the DSM unlike the FEM. The DSM has no limitation on the number of natural frequencies that can be computed. Thus it is significantly more computational efficient than the FEM.

The DSM has been largely developed for bars and beams [24–31] and implemented and validated in programs such as BUNVIS-RG [47] and PFVI-BAT [48].

The extension of the DSM to plate elements is essential to model complex aeronautical structures accurately. Wittrick and Williams [32–35] appear to be the first who attempted the extension of the DSM to plate elements and they achieved significant success. They implemented their dynamic stiffness theories into a program called VIPASA [35, 38, 39]. In the engineering literature, this program made considerable impact at the time and it was subsequently developed further. Foremost amongst these developments are VICON [38], PASCO [36, 37] and VICONOPT [31, 40–42] which are all well documented. The authors of this paper improved the DS plate theory developed by Wittrick and Williams by including the important effects of

shear deformation and rotatory inertia but their investigation was focused on isotropic plates [43]. In a parallel investigation, the authors also developed the corresponding DSM for inplane free vibratory motion of isotropic plates [44] wherein a set of previously missed inplane modes was identified. Following these earlier investigations, the DSM was extended by the authors to composite plates using the first order shear deformation theory (FSDT) see [45,46] and Reddy's high order shear deformation theory in [49]. Some application of the theory to aeronautical structures have been reported in [50]. These developments by the authors have been implemented in a computer program called DySAP.

In this paper, the extension of the DSM using a first order layer wise theory based on the CUF is presented, the results from the theory are validated and the superior accuracy is demonstrated. In Section (2) the fundamental equations of solid mechanics relevant to the investigation are presented. Next, CUF is used to derive the equations of motion and boundary conditions for one orthotropic layer in explicit form in the first instance. In section (3), a novel method, called the L -matrix method has been presented to obtain automatically the equations of motions and boundary condition of a plate with N_l number of layers. This is achieved through the use of a matrix \mathbf{L} which can be conveniently expanded and assembled. This is one of the most important contributions made by this paper because this novel method to write the equations of motion can be used for any problem for which the equation of motions depends on the analysis parameters. Subsequently, an algorithm to simultaneously solve the system of second order differential equations in an automatic way has been devised and presented. In section (4), the DSM for

the formulated problem is developed and the dynamic stiffness matrix of the element is obtained (section (4.1)). Assembly and boundary conditions are dealt with in sections (4.2) and (4.3) respectively. The Wittrick and Williams algorithm has been summarised in section (4.4) and an efficient procedure to obtain the mode shapes from as few as one element is presented in section (4.5). Given the complexity of the problem, a step by step procedure to obtain the DSM matrix for a layer wise formulation is given in section (5). In section (6), the developed formulation is first validate against Navier type solutions and then used to obtain closed form solution of multilayered composite plates with different boundary conditions which hitherto have not been obtained. These results can be used as benchmark for validating finite element and other approximate models. In the last section, some conclusions are drawn.

2. PRELIMINARIES: FROM PLATE MODEL TO GENERALISED EQUATIONS OF MOTION BY THE CARRERA'S UNIFIED FORMULATION (CUF)

The Carrera's Unified Formulation (CUF) [12, 14, 16, 17, 22, 23] has been used in this section to obtain the equations of motion and boundary conditions for a multilayered plate. The prerequisites needed to formulate the problem in the CUF notation can be summarised as:

- (i) Displacement assumptions (section (2.1));
- (ii) Geometrical equations (section (2.2));
- (iii) Constitutive equations (section (2.3));

The above details are substituted into Hamilton's principle to give a 3×3 matrix, often called the nucleus (section (2.4)), which can be conveniently expanded to the required plate theory depending on its order and assembled across the layers for composites to give either the FE stiffness matrix or the Navier's type analytical stiffness matrix of the system [12, 14, 16, 17, 22, 23]. The CUF nucleus, different from previously published, has been used to obtain the differential equations of motion of the system in this paper (section (2.5)).

2.1. Displacement formulation

The displacement field is formulated by using thickness functions $F_\tau(z)$ in order to reduce the 3D problem where the unknown displacements $\mathbf{u}(x, y, z, t) = \{u, v, w\}$ are function of x, y, z and t to a 2D problem for which the displacements are only function of 2 independent variables (x, y and t). By using the CUF, plate theories of any order (N_{CUF}) can be formulated by using a unified notation.

$$\mathbf{u}^k(x, y, z, t) = F_b(z)\mathbf{u}_b^k(x, y, t) + F_r(z)\mathbf{u}_r^k(x, y, t) + F_t(z)\mathbf{u}_t^k(x, y, t) \quad (1)$$

for $r = 2, \dots, N_{CUF} - 1$ where N_{CUF} is the order of the plate theory to be used and the superscript k refer to the layer number. Eq.(1) can be rewritten in a more compact form by making use of Einstein's notation where a double subscript stands for the usual summation

$$\mathbf{u}^k = F_\tau \mathbf{u}_\tau^k \quad (2)$$

The choice of the F_τ determines the type of theory to be used [12, 14, 16, 17, 22, 23]. In this study, a layer-wise formulation needs to be adopted, thus the

thickness function F_r take the form of Legendre's polynomials

$$F_t = \frac{P_0 + P_1}{2}, \quad F_b = \frac{P_0 - P_1}{2}, \quad F_r = P_r - P_{r-2} \quad r = 2, \dots, N \quad (3)$$

where $P_i(\zeta_k)$ is the i -order Legendre polynomial in the domain $-1 \leq \zeta_k \leq 1$ and $\zeta_k = z/h_k$. The first five Legendre polynomials are:

$$P_0 = 1 \quad P_1 = \zeta_k \quad P_2 = \frac{3\zeta_k^2 - 1}{2} \quad P_3 = \frac{5\zeta_k^3 - 3\zeta_k}{2} \quad P_4 = \frac{35\zeta_k^4 - 30\zeta_k^2 + 3}{8} \quad (4)$$

The choice of these functions is not arbitrary but they must satisfy the following fundamental properties:

$$\zeta_k = \begin{cases} 1 : & F_t = 1, \quad F_b = 0, \quad F_r = 0 \\ -1 : & F_t = 0, \quad F_b = 1, \quad F_r = 0 \end{cases} \quad (5)$$

which implies that. \mathbf{u}_t^k and \mathbf{u}_b^k are in fact the displacements at the top and bottom of the k^{th} layer (see Eq. (1)). This is important to ensure compatibility at the interfaces between layers without the need to use Lagrange multipliers but by simply assembling the stiffness terms (or differential equations) in the right order noting that:

$$\mathbf{u}_t^k = \mathbf{u}_b^{(k+1)}, \quad \text{with } k = 1, \dots, N_L - 1 \quad (6)$$

2.2. Geometrical equations: strain-displacement relationships

The strain $\boldsymbol{\varepsilon}$ for the k^{th} layer can written as

$$\boldsymbol{\varepsilon}^{kT} = \left[\varepsilon_{xx}, \varepsilon_{yy}, \varepsilon_{zz}, \varepsilon_{yz}, \varepsilon_{xz}, \varepsilon_{xy} \right]^k = \left[\varepsilon_1, \varepsilon_2, \varepsilon_3, \varepsilon_4, \varepsilon_5, \varepsilon_6 \right]^k \quad (7)$$

The above vector can be split into two, showing inplane strain $\boldsymbol{\varepsilon}_p = [\varepsilon_{xx}, \varepsilon_{yy}, \varepsilon_{xy}]$ and out of plane or normal strain $\boldsymbol{\varepsilon}_n = [\varepsilon_{xz}, \varepsilon_{yz}, \varepsilon_{zz}]$. Their relation to the displacements $\mathbf{u} = [u, v, w]$ can be written as

$$\boldsymbol{\varepsilon}_p^k = \mathbf{D}_p \mathbf{u}^k \quad , \quad \boldsymbol{\varepsilon}_n^k = (\mathbf{D}_{np} + \mathbf{D}_{nz}) \mathbf{u}^k \quad (8)$$

where the differential or partial derivative matrices can be written as:

$$\mathbf{D}_p = \begin{bmatrix} \partial_x & 0 & 0 \\ 0 & \partial_y & 0 \\ \partial_y & \partial_x & 0 \end{bmatrix}, \mathbf{D}_{np} = \begin{bmatrix} 0 & 0 & \partial_x \\ 0 & 0 & \partial_y \\ 0 & 0 & 0 \end{bmatrix}, \mathbf{D}_{nz} = \begin{bmatrix} \partial_z & 0 & 0 \\ 0 & \partial_z & 0 \\ 0 & 0 & \partial_z \end{bmatrix} \quad (9)$$

with $\partial_x = \partial/\partial x$, $\partial_y = \partial/\partial y$, $\partial_z = \partial/\partial z$.

2.3. Constitutive equations: stress-strain relations

The complete 3D constitutive equations are used since thickness locking is generally not present for layer wise theories [51]. The stresses $\boldsymbol{\sigma}^k$ are

$$\boldsymbol{\sigma}^{kT} = \left[\sigma_{xx}, \sigma_{yy}, \sigma_{zz}, \sigma_{yz}, \sigma_{xz}, \sigma_{xy} \right]^k = \left[\sigma_1, \sigma_2, \sigma_3, \sigma_4, \sigma_5, \sigma_6 \right]^k \quad (10)$$

are related to the strain in the global reference system for orthotropic materials by

$$\boldsymbol{\sigma}_p^k = \mathbf{C}_{pp}^k \boldsymbol{\varepsilon}_p^k + \mathbf{C}_{pn}^k \boldsymbol{\varepsilon}_n^k, \quad \boldsymbol{\sigma}_n^k = \mathbf{C}_{pn}^{kT} \boldsymbol{\varepsilon}_p^k + \mathbf{C}_{nn}^k \boldsymbol{\varepsilon}_n^k \quad (11)$$

where

$$\mathbf{C}_{pp}^k = \begin{bmatrix} C_{11} & C_{12} & C_{16} \\ C_{12} & C_{22} & C_{26} \\ C_{16} & C_{26} & C_{66} \end{bmatrix}^k, \quad \mathbf{C}_{pn}^k = \begin{bmatrix} 0 & 0 & C_{13} \\ 0 & 0 & C_{23} \\ 0 & 0 & C_{36} \end{bmatrix}^k, \quad \mathbf{C}_{nn}^k = \begin{bmatrix} C_{55} & C_{45} & 0 \\ C_{45} & C_{44} & 0 \\ 0 & 0 & C_{33} \end{bmatrix}^k \quad (12)$$

$$\boldsymbol{\sigma}_p^{kT} = \left[\sigma_1, \sigma_2, \sigma_6 \right]^k, \quad \boldsymbol{\sigma}_n^{kT} = \left[\sigma_5, \sigma_4, \sigma_3 \right]^k \quad (13)$$

$$\boldsymbol{\varepsilon}_p^{kT} = \left[\varepsilon_1, \varepsilon_2, \varepsilon_6 \right]^k, \quad \boldsymbol{\varepsilon}_n^{kT} = \left[\varepsilon_5, \varepsilon_4, \varepsilon_3 \right]^k \quad (14)$$

The explicit expressions of the material properties for an orthotropic material in the lamina reference system and the rotation matrices to obtain the ones in the global coordinate system are presented in (APPENDIX A).

2.4. Developing CUF nucleus K

Once the model and the governing equation have been formulated, Hamilton's principle can now be used to obtain the equations of motion. The principle can be written by using the matrix form of the equations as

$$\sum_{k=1}^{N_l} \int_{A_k} \int_{h_k} \left\{ \delta \boldsymbol{\varepsilon}_{pG}^k T \boldsymbol{\sigma}_{pC}^k + \delta \boldsymbol{\varepsilon}_{nG}^k T \boldsymbol{\sigma}_{nC}^k \right\} dA_k dz = \delta \mathcal{L}_e - \delta \mathcal{L}_{in} \quad (15)$$

where \mathcal{L}_{in} is the work done by the inertia forces and \mathcal{L}_e by the external forces. In order to obtain the fundamental nucleus the following substitution into Eq. (15) should be made:

- (i) Constitutive relations Eq. (11) ;
- (ii) Geometric relations Eq. (8);
- (iii) Displacement formulation Eq. (2);

Finally by developing the matrix products and integrating by part equations of motion and natural boundary conditions are obtained. For the sake of brevity each single step is not reported here. The final result is a system of equations in matrix form so that

$$\mathbf{K}^{k\tau s} \mathbf{u}_s^k + \mathbf{M}^{k\tau s} \ddot{\mathbf{u}}_s^k = 0 \quad (16)$$

and the natural boundary conditions

$$\mathbf{u}_\tau^k = \bar{\mathbf{u}}_\tau^k \quad \text{or} \quad \mathbf{\Pi}_d^{k\tau s} \mathbf{u}_s^k = \bar{\mathbf{F}}_\tau^k \quad (17)$$

where τ and s are indexes which go from 1 to the order of the chosen formulation, i.e. the order of expansion of the displacement polynomials.

The matrix $\mathbf{K}^{k\tau s}$ is the CUF fundamental nucleus, i.e. a 3×3 matrix which,

when properly assembled through the thickness for different layers, gives the equations of motion of the plate.

$$\begin{aligned}
\mathbf{K}^{k\tau s} = \int_{A_k} \{ & - \mathbf{D}_p^T \mathbf{C}_{pp}^k \mathbf{D}_p \mathbf{I} E_{\tau s} - \mathbf{D}_p^T \mathbf{C}_{pn}^k \mathbf{D}_{np} \mathbf{I} E_{\tau s} - \mathbf{D}_p^T \mathbf{C}_{pn}^k \mathbf{I} E_{\tau s, z} \\
& - \mathbf{D}_{np}^T \mathbf{C}_{pn}^{kT} \mathbf{D}_p \mathbf{I} E_{\tau s} - \mathbf{D}_{np}^T \mathbf{C}_{nn}^k \mathbf{D}_{np} \mathbf{I} E_{\tau s} - \mathbf{D}_{np}^T \mathbf{C}_{nn}^k \mathbf{I} E_{\tau s, z} \\
& + \mathbf{C}_{pn}^{kT} \mathbf{D}_p \mathbf{I} E_{\tau, z s} + \mathbf{C}_{nn}^k \mathbf{D}_{np} \mathbf{I} E_{\tau, z s} + \mathbf{C}_{nn}^k \mathbf{I} E_{\tau, z s, z} \} dz
\end{aligned} \tag{18}$$

The matrix $\mathbf{M}^{k\tau s}$ is the mass matrix (shown below), which needs to be assembled across the layers just like the stiffness matrix $\mathbf{K}^{k\tau s}$.

$$\mathbf{M}^{k\tau s} = \int_{A_k} \{ \rho^k \mathbf{I} E_{\tau s} \} dz \tag{19}$$

The boundary conditions are formulated by 3×1 vector which needs to be assembled as well.

$$\begin{aligned}
\mathbf{\Pi}^{k\tau s} = \int_{A_k} \{ & \mathbf{I}_p^T \mathbf{C}_{pp}^k \mathbf{D}_p \mathbf{I} E_{\tau s} + \mathbf{I}_p^T \mathbf{C}_{pn}^k \mathbf{D}_{np} \mathbf{I} E_{\tau s} + \mathbf{I}_p^T \mathbf{C}_{pn}^k \mathbf{I} E_{\tau s, z} \\
& + \mathbf{I}_{np}^T \mathbf{C}_{pn}^{kT} \mathbf{D}_p \mathbf{I} E_{\tau s} + \mathbf{I}_{np}^T \mathbf{C}_{nn}^k \mathbf{D}_{np} \mathbf{I} E_{\tau s} + \mathbf{I}_{np}^T \mathbf{C}_{nn}^k \mathbf{I} E_{\tau s, z} \} dz
\end{aligned} \tag{20}$$

With regard to the boundary condition equations which come from the integration by part, it is necessary to develop a method to keep track of the edge on which they need to be computed (either $x = 0, b$ or $y = 0, L$). Two coefficients Γ_b and Γ_L are used to represent ∂_x and ∂_y respectively. By putting one of the coefficient to 1 and the other to 0, the boundary conditions on the two different edges can be obtained from the same formulation. In order to

achieve this, the following matrices are used:

$$\mathbf{I} = \begin{bmatrix} 1 & 0 & 0 \\ 0 & 1 & 0 \\ 0 & 0 & 1 \end{bmatrix}, \mathbf{I}_p = \begin{bmatrix} \Gamma_b & 0 & 0 \\ 0 & \Gamma_L & 0 \\ \Gamma_L & \Gamma_b & 0 \end{bmatrix}, \mathbf{I}_{np} = \begin{bmatrix} 0 & 0 & \Gamma_b \\ 0 & 0 & \Gamma_L \\ 0 & 0 & 0 \end{bmatrix} \quad (21)$$

The integrals through the thickness are written as:

$$\begin{aligned} \mathbf{E}_{\tau s} &= \int_{h_k} F_\tau F_s dz & \mathbf{E}_{\tau,zs} &= \int_{h_k} F_{\tau,z} F_s dz \\ \mathbf{E}_{\tau s,z} &= \int_{h_k} F_\tau F_{s,z} dz & \mathbf{E}_{\tau,zs,z} &= \int_{h_k} F_{\tau,z} F_{s,z} dz \end{aligned} \quad (22)$$

Thus the explicit terms of the fundamental nucleus can be written as

$$\begin{aligned} K^{k\tau s}_{11} &= (-C_{11}^k \partial_x^2 - 2C_{16}^k \partial_x \partial_y - C_{66}^k \partial_y^2) E_{\tau s} + C_{55}^k E_{\tau,zs,z} \\ K^{k\tau s}_{12} &= (-C_{16}^k \partial_x^2 - (C_{12}^k + C_{66}^k) \partial_x \partial_y - C_{26}^k \partial_y^2) E_{\tau s} + C_{45}^k E_{\tau,zs,z} \\ K^{k\tau s}_{13} &= (C_{55}^k \partial_x + C_{45}^k \partial_y) E_{\tau,zs} - (C_{13}^k \partial_x + C_{36}^k \partial_y) E_{\tau s,z} \\ K^{k\tau s}_{21} &= (-C_{16}^k \partial_x^2 - (C_{12}^k + C_{66}^k) \partial_x \partial_y - C_{26}^k \partial_y^2) E_{\tau s} + C_{45}^k E_{\tau,zs,z} \\ K^{k\tau s}_{22} &= (-C_{66}^k \partial_x^2 - 2C_{26}^k \partial_x \partial_y - C_{22}^k \partial_y^2) E_{\tau s} + C_{44}^k E_{\tau,zs,z} \\ K^{k\tau s}_{23} &= (C_{45}^k \partial_x + C_{44}^k \partial_y) E_{\tau,zs} - (C_{36}^k \partial_x + C_{23}^k \partial_y) E_{\tau s,z} \\ K^{k\tau s}_{31} &= (C_{13}^k \partial_x + C_{36}^k \partial_y) E_{\tau,zs} - (C_{55}^k \partial_x + C_{45}^k \partial_y) E_{\tau s,z} \\ K^{k\tau s}_{32} &= (C_{36}^k \partial_x + C_{23}^k \partial_y) E_{\tau,zs} - (C_{45}^k \partial_x + C_{44}^k \partial_y) E_{\tau s,z} \\ K^{k\tau s}_{33} &= (-C_{55}^k \partial_x^2 - 2C_{45}^k \partial_x \partial_y - C_{44}^k \partial_y^2) E_{\tau s} + C_{33}^k E_{\tau,zs,z} \end{aligned} \quad (23)$$

$$\begin{aligned} K^{k\tau s}_{11} &= K^{k\tau s}_{22} = K^{k\tau s}_{33} = \rho^k E_{\tau s} \\ K^{k\tau s}_{12} &= K^{k\tau s}_{13} = K^{k\tau s}_{21} = K^{k\tau s}_{23} = K^{k\tau s}_{31} = K^{k\tau s}_{32} = 0 \end{aligned} \quad (24)$$

and the boundary conditions are:

$$\begin{aligned}
\Pi^{k\tau s}_{11} &= (\partial_x(\Gamma_b C_{11}^k + \Gamma_L C_{16}^k) + \partial_y(\Gamma_b C_{16}^k + \Gamma_L C_{66}^k)) E_{\tau s} \\
\Pi^{k\tau s}_{12} &= (\partial_x(\Gamma_b C_{16}^k + \Gamma_L C_{66}^k) + \partial_y(\Gamma_b C_{12}^k + \Gamma_L C_{26}^k)) E_{\tau s} \\
\Pi^{k\tau s}_{13} &= (\Gamma_b C_{13}^k + \Gamma_L C_{36}^k) E_{\tau s, z} \\
\Pi^{k\tau s}_{21} &= (\partial_x(\Gamma_L C_{12}^k + \Gamma_b C_{16}^k) + \partial_y(\Gamma_L C_{26}^k + \Gamma_b C_{66}^k)) E_{\tau s} \\
\Pi^{k\tau s}_{22} &= (\partial_x(\Gamma_L C_{26}^k + \Gamma_b C_{66}^k) + \partial_y(\Gamma_L C_{22}^k + \Gamma_b C_{26}^k)) E_{\tau s} \\
\Pi^{k\tau s}_{23} &= (\Gamma_L C_{23}^k + \Gamma_b C_{36}^k) E_{\tau s, z} \\
\Pi^{k\tau s}_{31} &= (\Gamma_L C_{45}^k + \Gamma_b C_{55}^k) E_{\tau s, z} \\
\Pi^{k\tau s}_{32} &= (\Gamma_L C_{44}^k + \Gamma_b C_{45}^k) E_{\tau s, z} \\
\Pi^{k\tau s}_{33} &= (\partial_x(\Gamma_L C_{45}^k + \Gamma_b C_{55}^k) + \partial_y(\Gamma_L C_{44}^k + \Gamma_b C_{45}^k)) E_{\tau s}
\end{aligned} \tag{25}$$

2.5. General equations of motion for first order layer wise plate theory, LD1

By using the CUF, any order of expansion, i.e. any higher order plate theory can be obtained by suitably expanding the indexes τ and s in Eq. (23). In this study, the expansion is limited to the first order and thus, the indexes τ and s will simply refer to the bottom b and top t interfaces of the k^{th} layer. This formulation is usually referred to in the literature as LD1 [12, 14, 16, 17, 22, 23]. The displacement functions, by referring to Eq. (1), can be written as

$$\mathbf{u}^k(x, y, z, t) = F_b(z) \mathbf{u}_b^k(x, y, t) + F_t(z) \mathbf{u}_t^k(x, y, t) \tag{26}$$

where the thickness functions (see Eq. (3)) can be written as

$$F_t = \frac{1}{2} - \frac{z}{h}, \quad F_b = \frac{1}{2} + \frac{z}{h}, \tag{27}$$

and

$$\mathbf{u}_b^k = [u_b^k, v_b^k, w_b^k]^T, \quad \mathbf{u}_t^k = [u_t^k, v_t^k, w_t^k]^T \tag{28}$$

Once the displacement formulation has been chosen as the one related to Eq. (26) and (27) the nuclei can be obtained by using equations (18) and (23) by computing the integrals in Eq. (22). For the k^{th} layer, the nucleus can be split into four 3×3 submatrices which will be referred to as \mathbf{K}_{bb}^k , \mathbf{K}_{bt}^k , \mathbf{K}_{tb}^k , \mathbf{K}_{tt}^k . Also the mass matrix can be computed from Eq. (19) and (24) in the same way to give \mathbf{M}_{bb}^k , \mathbf{M}_{bt}^k , \mathbf{M}_{tb}^k , \mathbf{M}_{tt}^k .

$$\mathbf{K}^{k\tau s} \mathbf{u}_s^k + \mathbf{M}^{k\tau s} \ddot{\mathbf{u}}_s^k = 0 \quad (29)$$

Equation (29) can be written explicitly as 6 differential equations of motion. These 6 differential equations describe the behaviour of only 1 layer using a first order layer wise plate formulation called LD1.

$$\begin{aligned} & + \left(\frac{C_{55}^k}{h^k} - \frac{1}{3} h^k \left(C_{11}^k \frac{\partial^2}{\partial x^2} + 2C_{16}^k \frac{\partial^2}{\partial x \partial y} + C_{66}^k \frac{\partial^2}{\partial y^2} \right) \right) u_b^k \\ & - \left(\frac{C_{55}^k}{h^k} + \frac{1}{6} h^k \left(C_{11}^k \frac{\partial^2}{\partial x^2} + 2C_{16}^k \frac{\partial^2}{\partial x \partial y} + C_{66}^k \frac{\partial^2}{\partial y^2} \right) \right) u_t^k \\ & + \left(\frac{C_{45}^k}{h^k} - \frac{1}{3} h^k \left(C_{16}^k \frac{\partial^2}{\partial x^2} + (C_{12}^k + C_{66}^k) \frac{\partial^2}{\partial x \partial y} + C_{26}^k \frac{\partial^2}{\partial y^2} \right) \right) v_b^k \\ & - \left(\frac{C_{45}^k}{h^k} + \frac{1}{6} h^k \left(C_{16}^k \frac{\partial^2}{\partial x^2} + (C_{12}^k + C_{66}^k) \frac{\partial^2}{\partial x \partial y} + C_{26}^k \frac{\partial^2}{\partial y^2} \right) \right) v_t^k \quad (30) \\ & + \frac{1}{2} \left((C_{13}^k - C_{55}^k) \frac{\partial}{\partial x} + (C_{36}^k - C_{45}^k) \frac{\partial}{\partial y} \right) w_b^k \\ & - \frac{1}{2} \left((C_{13}^k + C_{55}^k) \frac{\partial}{\partial x} + (C_{36}^k + C_{45}^k) \frac{\partial}{\partial y} \right) w_t^k \\ & + \frac{1}{3} h^k \rho^k \frac{\partial^2 u_b^k}{\partial t^2} + \frac{1}{6} h^k \rho^k \frac{\partial^2 u_t^k}{\partial t^2} = 0 \end{aligned}$$

$$\begin{aligned} & + \left(\frac{C_{45}^k}{h^k} - \frac{1}{3} h^k \left(C_{16}^k \frac{\partial^2}{\partial x^2} + (C_{12}^k + C_{66}^k) \frac{\partial^2}{\partial x \partial y} + C_{26}^k \frac{\partial^2}{\partial y^2} \right) \right) u_b^k \\ & - \left(\frac{C_{45}^k}{h^k} + \frac{1}{6} h^k \left(C_{16}^k \frac{\partial^2}{\partial x^2} + (C_{12}^k + C_{66}^k) \frac{\partial^2}{\partial x \partial y} + C_{26}^k \frac{\partial^2}{\partial y^2} \right) \right) u_t^k \\ & + \left(\frac{C_{44}^k}{h^k} - \frac{1}{3} h^k \left(C_{66}^k \frac{\partial^2}{\partial x^2} + 2C_{26}^k \frac{\partial^2}{\partial x \partial y} + C_{22}^k \frac{\partial^2}{\partial y^2} \right) \right) v_b^k \\ & - \left(\frac{C_{44}^k}{h^k} + \frac{1}{6} h^k \left(C_{66}^k \frac{\partial^2}{\partial x^2} + 2C_{26}^k \frac{\partial^2}{\partial x \partial y} + C_{22}^k \frac{\partial^2}{\partial y^2} \right) \right) v_t^k \quad (31) \\ & + \frac{1}{2} \left((C_{36}^k - C_{45}^k) \frac{\partial}{\partial x} + (C_{23}^k - C_{44}^k) \frac{\partial}{\partial y} \right) w_b^k \\ & - \frac{1}{2} \left((C_{36}^k + C_{45}^k) \frac{\partial}{\partial x} + (C_{23}^k + C_{44}^k) \frac{\partial}{\partial y} \right) w_t^k \\ & + \frac{1}{3} h^k \rho^k \frac{\partial^2 v_b^k}{\partial t^2} + \frac{1}{6} h^k \rho^k \frac{\partial^2 v_t^k}{\partial t^2} = 0 \end{aligned}$$

$$\begin{aligned}
& +\frac{1}{2} \left((C_{55}^k - C_{13}^k) \frac{\partial}{\partial x} + (C_{45}^k - C_{36}^k) \frac{\partial}{\partial y} \right) & u_b^k \\
& -\frac{1}{2} \left((C_{55}^k + C_{13}^k) \frac{\partial}{\partial x} + (C_{45}^k + C_{36}^k) \frac{\partial}{\partial y} \right) & u_t^k \\
& +\frac{1}{2} \left((C_{45}^k - C_{36}^k) \frac{\partial}{\partial x} + (C_{44}^k - C_{23}^k) \frac{\partial}{\partial y} \right) & v_b^k \\
& -\frac{1}{2} \left((C_{45}^k + C_{36}^k) \frac{\partial}{\partial x} + (C_{44}^k + C_{23}^k) \frac{\partial}{\partial y} \right) & v_t^k \\
& + \left(\frac{C_{33}^k}{h^k} - \frac{1}{3} h^k \left(C_{55}^k \frac{\partial^2}{\partial x^2} + 2C_{45}^k \frac{\partial^2}{\partial x \partial y} + C_{44}^k \frac{\partial^2}{\partial y^2} \right) \right) & w_b^k \\
& - \left(\frac{C_{33}^k}{h^k} + \frac{1}{6} h^k \left(C_{55}^k \frac{\partial^2}{\partial x^2} + 2C_{45}^k \frac{\partial^2}{\partial x \partial y} + C_{44}^k \frac{\partial^2}{\partial y^2} \right) \right) & w_t^k \\
& +\frac{1}{3} h^k \rho^k \frac{\partial^2 w_b^k}{\partial t^2} + \frac{1}{6} h^k \rho^k \frac{\partial^2 w_t^k}{\partial t^2} = 0
\end{aligned} \tag{32}$$

$$\begin{aligned}
& - \left(\frac{C_{55}^k}{h^k} + \frac{1}{6} h^k \left(C_{11}^k \frac{\partial^2}{\partial x^2} + 2C_{16}^k \frac{\partial^2}{\partial x \partial y} + C_{66}^k \frac{\partial^2}{\partial y^2} \right) \right) & u_b^k \\
& + \left(\frac{C_{55}^k}{h^k} - \frac{1}{3} h^k \left(C_{11}^k \frac{\partial^2}{\partial x^2} + 2C_{16}^k \frac{\partial^2}{\partial x \partial y} + C_{66}^k \frac{\partial^2}{\partial y^2} \right) \right) & u_t^k \\
& - \left(\frac{C_{45}^k}{h^k} + \frac{1}{6} h^k \left(C_{16}^k \frac{\partial^2}{\partial x^2} + (C_{12}^k + C_{66}^k) \frac{\partial^2}{\partial x \partial y} + C_{26}^k \frac{\partial^2}{\partial y^2} \right) \right) & v_b^k \\
& + \left(\frac{C_{45}^k}{h^k} - \frac{1}{6} h^k \left(C_{16}^k \frac{\partial^2}{\partial x^2} + (C_{12}^k + C_{66}^k) \frac{\partial^2}{\partial x \partial y} + C_{26}^k \frac{\partial^2}{\partial y^2} \right) \right) & v_t^k \\
& +\frac{1}{2} \left((C_{13}^k + C_{55}^k) \frac{\partial}{\partial x} + (C_{36}^k + C_{45}^k) \frac{\partial}{\partial y} \right) & w_b^k \\
& -\frac{1}{2} \left((C_{13}^k - C_{55}^k) \frac{\partial}{\partial x} + (C_{36}^k - C_{45}^k) \frac{\partial}{\partial y} \right) & w_t^k \\
& +\frac{1}{6} h^k \rho^k \frac{\partial^2 u_b^k}{\partial t^2} + \frac{1}{3} h^k \rho^k \frac{\partial^2 u_t^k}{\partial t^2} = 0
\end{aligned} \tag{33}$$

$$\begin{aligned}
& - \left(\frac{C_{45}^k}{h^k} + \frac{1}{6} h^k \left(C_{16}^k \frac{\partial^2}{\partial x^2} + (C_{12}^k + C_{66}^k) \frac{\partial^2}{\partial x \partial y} + C_{26}^k \frac{\partial^2}{\partial y^2} \right) \right) & u_b^k \\
& + \left(\frac{C_{45}^k}{h^k} - \frac{1}{3} h^k \left(C_{16}^k \frac{\partial^2}{\partial x^2} + (C_{12}^k + C_{66}^k) \frac{\partial^2}{\partial x \partial y} + C_{26}^k \frac{\partial^2}{\partial y^2} \right) \right) & u_t^k \\
& - \left(\frac{C_{44}^k}{h^k} + \frac{1}{6} h^k \left(C_{66}^k \frac{\partial^2}{\partial x^2} + 2C_{26}^k \frac{\partial^2}{\partial x \partial y} + C_{22}^k \frac{\partial^2}{\partial y^2} \right) \right) & v_b^k \\
& + \left(\frac{C_{44}^k}{h^k} - \frac{1}{3} h^k \left(C_{66}^k \frac{\partial^2}{\partial x^2} + 2C_{26}^k \frac{\partial^2}{\partial x \partial y} + C_{22}^k \frac{\partial^2}{\partial y^2} \right) \right) & v_t^k \\
& +\frac{1}{2} \left((C_{36}^k + C_{45}^k) \frac{\partial}{\partial x} + (C_{23}^k + C_{44}^k) \frac{\partial}{\partial y} \right) & w_b^k \\
& -\frac{1}{2} \left((C_{36}^k - C_{45}^k) \frac{\partial}{\partial x} + (C_{23}^k - C_{44}^k) \frac{\partial}{\partial y} \right) & w_t^k \\
& +\frac{1}{6} h^k \rho^k \frac{\partial^2 v_b^k}{\partial t^2} + \frac{1}{3} h^k \rho^k \frac{\partial^2 v_t^k}{\partial t^2} = 0
\end{aligned} \tag{34}$$

$$\begin{aligned}
& +\frac{1}{2} \left((C_{55}^k + C_{13}^k) \frac{\partial}{\partial x} + (C_{45}^k + C_{36}^k) \frac{\partial}{\partial y} \right) u_b^k \\
& -\frac{1}{2} \left((C_{55}^k - C_{13}^k) \frac{\partial}{\partial x} + (C_{45}^k - C_{36}^k) \frac{\partial}{\partial y} \right) u_t^k \\
& +\frac{1}{2} \left((C_{45}^k + C_{36}^k) \frac{\partial}{\partial x} + (C_{44}^k + C_{23}^k) \frac{\partial}{\partial y} \right) v_b^k \\
& -\frac{1}{2} \left((C_{45}^k - C_{36}^k) \frac{\partial}{\partial x} + (C_{44}^k - C_{23}^k) \frac{\partial}{\partial y} \right) v_t^k \\
& - \left(\frac{C_{33}^k}{h^k} + \frac{1}{6} h^k \left(C_{55}^k \frac{\partial^2}{\partial x^2} + 2C_{45}^k \frac{\partial^2}{\partial x \partial y} + C_{44}^k \frac{\partial^2}{\partial y^2} \right) \right) w_b^k \\
& + \left(\frac{C_{33}^k}{h^k} - \frac{1}{3} h^k \left(C_{55}^k \frac{\partial^2}{\partial x^2} + 2C_{45}^k \frac{\partial^2}{\partial x \partial y} + C_{44}^k \frac{\partial^2}{\partial y^2} \right) \right) w_t^k \\
& + \frac{1}{6} h^k \rho^k \frac{\partial^2 w_b^k}{\partial t^2} + \frac{1}{3} h^k \rho^k \frac{\partial^2 w_t^k}{\partial t^2} = 0
\end{aligned} \tag{35}$$

and the boundary condition can be written explicitly by using Eqs. (20) and (25) and putting $\Gamma_L = 0$ and $\Gamma_b = 1$ to limit our focus to the sides at $x = 0$ and $x = b$.

$$\begin{aligned}
F_{u_b} = & +\frac{1}{3} h^k \left(C_{11}^k \frac{\partial}{\partial x} + C_{16}^k \frac{\partial}{\partial y} \right) u_b^k + \frac{1}{6} h^k \left(C_{11}^k \frac{\partial}{\partial x} + C_{16}^k \frac{\partial}{\partial y} \right) u_t^k \\
& +\frac{1}{3} h^k \left(C_{16}^k \frac{\partial}{\partial x} + C_{12}^k \frac{\partial}{\partial y} \right) v_b^k + \frac{1}{6} h^k \left(C_{16}^k \frac{\partial}{\partial x} + C_{12}^k \frac{\partial}{\partial y} \right) v_t^k \\
& -\frac{C_{13}^k}{2} w_b^k + \frac{C_{13}^k}{2} w_t^k
\end{aligned} \tag{36}$$

$$\begin{aligned}
F_{v_b} = & +\frac{1}{3} h^k \left(C_{16}^k \frac{\partial}{\partial x} + C_{66}^k \frac{\partial}{\partial y} \right) u_b^k + \frac{1}{6} h^k \left(C_{16}^k \frac{\partial}{\partial x} + C_{66}^k \frac{\partial}{\partial y} \right) u_t^k \\
& +\frac{1}{3} h^k \left(C_{66}^k \frac{\partial}{\partial x} + C_{26}^k \frac{\partial}{\partial y} \right) v_b^k + \frac{1}{6} h^k \left(C_{66}^k \frac{\partial}{\partial x} + C_{26}^k \frac{\partial}{\partial y} \right) v_t^k \\
& -\frac{C_{36}^k}{2} w_b^k + \frac{C_{36}^k}{2} w_t^k
\end{aligned} \tag{37}$$

$$\begin{aligned}
F_{w_b} = & -\frac{C_{55}^k}{2} u_b^k + \frac{C_{55}^k}{2} u_t^k - \frac{C_{45}^k}{2} v_b^k + \frac{C_{45}^k}{2} v_t^k \\
& +\frac{1}{3} h^k \left(C_{55}^k \frac{\partial}{\partial x} + C_{45}^k \frac{\partial}{\partial y} \right) w_b^k + \frac{1}{6} h^k \left(C_{55}^k \frac{\partial}{\partial x} + C_{45}^k \frac{\partial}{\partial y} \right) w_t^k
\end{aligned} \tag{38}$$

$$\begin{aligned}
F_{u_b} = & +\frac{1}{6} h^k \left(C_{11}^k \frac{\partial}{\partial x} + C_{16}^k \frac{\partial}{\partial y} \right) u_b^k + \frac{1}{3} h^k \left(C_{11}^k \frac{\partial}{\partial x} + C_{16}^k \frac{\partial}{\partial y} \right) u_t^k \\
& +\frac{1}{6} h^k \left(C_{16}^k \frac{\partial}{\partial x} + C_{12}^k \frac{\partial}{\partial y} \right) v_b^k + \frac{1}{3} h^k \left(C_{16}^k \frac{\partial}{\partial x} + C_{12}^k \frac{\partial}{\partial y} \right) v_t^k \\
& -\frac{C_{13}^k}{2} w_b^k + \frac{C_{13}^k}{2} w_t^k
\end{aligned} \tag{39}$$

$$\begin{aligned}
F_{v_b} = & +\frac{1}{6}h^k \left(C_{16}^k \frac{\partial}{\partial x} + C_{66}^k \frac{\partial}{\partial y} \right) u_b^k + \frac{1}{3}h^k \left(C_{16}^k \frac{\partial}{\partial x} + C_{66}^k \frac{\partial}{\partial y} \right) u_t^k \\
& +\frac{1}{6}h^k \left(C_{66}^k \frac{\partial}{\partial x} + C_{26}^k \frac{\partial}{\partial y} \right) v_b^k + \frac{1}{3}h^k \left(C_{66}^k \frac{\partial}{\partial x} + C_{26}^k \frac{\partial}{\partial y} \right) v_t^k \\
& -\frac{C_{36}^k}{2}w_b^k + \frac{C_{36}^k}{2}w_t^k
\end{aligned} \tag{40}$$

$$\begin{aligned}
F_{w_b} = & -\frac{C_{55}^k}{2}u_b^k + \frac{C_{55}^k}{2}u_t^k & -\frac{C_{45}^k}{2}v_b^k + \frac{C_{45}^k}{2}v_t^k \\
& +\frac{1}{6}h^k \left(C_{55}^k \frac{\partial}{\partial x} + C_{45}^k \frac{\partial}{\partial y} \right) w_b^k & +\frac{1}{3}h^k \left(C_{55}^k \frac{\partial}{\partial x} + C_{45}^k \frac{\partial}{\partial y} \right) w_t^k
\end{aligned} \tag{41}$$

Sign convention for forces and displacements are shown in Figure (3).

The above system of quadratic, fully coupled, constant coefficient partial differential equations needs to be solved simultaneously along with the BC to obtain the solution for 1 layer.

If the solution for 2 layers is sought, the equations need to be recalculated and rewritten from the beginning and thus making it a very difficult task. For two layers, 9 equations (3 for each interface) would be obtained. For this reasons the author devised a method, inspired by the CUF, to automatically assemble the differential equation of motions (*not* the stiffness matrices) and BCs for any number of layers and automatically solve them. This method has been called the **L** matrix method which makes use in a particular way to write the equations for 1 layer so that they can be assembled for several layers and solved automatically. Before tackling that problem though, the partial derivatives need to be transformed to ordinary derivatives in order to be able to solve them simultaneously.

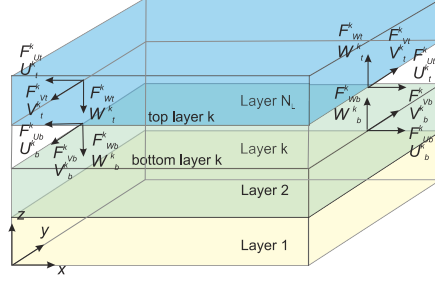


Figure 3: Coordinate system and notations for displacements and forces for a multilayered plate.

2.6. *From partial to ordinary differential equations for plates with two opposite sides simply supported*

The system of partial differential equations for 1 layer can be reduced to a set of ordinary ones (one for each m) by making use of *sin* waves in the y direction and the exponential function for the time t . Thus

$$\begin{aligned}
 u_b^k(x, y, t) &= \sum_{m=1}^{\infty} U_b^k(x) \sin(\alpha_m y) e^{i\omega t}; & u_t^k(x, y, t) &= \sum_{m=1}^{\infty} U_t^k(x) \sin(\alpha_m y) e^{i\omega t} \\
 v_b^k(x, y, t) &= \sum_{m=1}^{\infty} V_b^k(x) \cos(\alpha_m y) e^{i\omega t}; & v_t^k(x, y, t) &= \sum_{m=1}^{\infty} V_t^k(x) \cos(\alpha_m y) e^{i\omega t} \\
 w_b^k(x, y, t) &= \sum_{m=1}^{\infty} W_b^k(x) \sin(\alpha_m y) e^{i\omega t}; & w_t^k(x, y, t) &= \sum_{m=1}^{\infty} W_t^k(x) \sin(\alpha_m y) e^{i\omega t}
 \end{aligned} \tag{42}$$

where ω is an arbitrary circular or angular frequency, $\alpha_m = \frac{m\pi}{L}$ and $m = 1, 2, \dots, \infty$. This is also referred to in the literature as Levy's solution and complies with the boundary condition associated to a plate where the two sides $y=0$ and $y=L$ are simply supported (SS) (i.e. $u_b^k = w_b^k = u_t^k = w_t^k = 0$ at $y = 0$ and $y = L$). By substituting Eq. (42) into the Eqs. (30)-(35), and

assuming to study a material for which, $C_{16}^k = C_{26}^k = C_{36}^k = C_{45}^k = 0^1$ (i.e. either 0 or 90 degree ply for composite plates) the following system of fully coupled, quadratic, ordinary differential equations can be written as

$$\begin{cases} \frac{a_1+3C_{55}^k}{3h^k}U_b + \frac{a_1-6C_{55}^k}{6h^k}U_t + \frac{a_2}{3h^k}V_b' + \frac{a_2}{6h^k}V_t' + \frac{a_3}{6h^k}W_b' + \frac{a_4}{6h^k}W_t' - \frac{1}{3}C_{11}^kh^kU_b'' - \frac{1}{6}C_{11}^kh^kU_t'' & = 0 \\ -\frac{2a_5-6C_{44}^k}{6h^k}V_b - \frac{a_5+6C_{44}^k}{6h^k}V_t + \frac{a_7}{6h^k}W_b + \frac{a_6}{6h^k}W_t - \frac{a_2}{3h^k}U_b' - \frac{a_2}{6h^k}U_t' - \frac{1}{3}C_{66}^kh^kV_b'' - \frac{1}{6}C_{66}^kh^kV_t'' & = 0 \\ \frac{a_7}{6h^k}V_b - \frac{a_6}{6h^k}V_t - \frac{2a_8-6C_{33}^k}{6h^k}W_b - \frac{a_8+6C_{33}^k}{6h^k}W_t - \frac{a_3}{6h^k}U_b' + \frac{a_4}{6h^k}U_t' - \frac{1}{3}C_{55}^kh^kW_b'' - \frac{1}{6}C_{55}^kh^kW_t'' & = 0 \\ \frac{a_1-6C_{55}^k}{3h^k}U_b + \frac{a_1+3C_{55}^k}{6h^k}U_t + \frac{a_2}{6h^k}V_b' + \frac{a_2}{3h^k}V_t' - \frac{a_4}{6h^k}W_b' - \frac{a_3}{6h^k}W_t' - \frac{1}{6}C_{11}^kh^kU_b'' - \frac{1}{3}C_{11}^kh^kU_t'' & = 0 \\ -\frac{a_5+6C_{44}^k}{6h^k}V_b - \frac{2a_5-6C_{44}^k}{6h^k}V_t - \frac{a_6}{6h^k}W_b - \frac{a_7}{6h^k}W_t - \frac{a_2}{6h^k}U_b' - \frac{a_2}{3h^k}U_t' - \frac{1}{6}C_{66}^kh^kV_b'' - \frac{1}{3}C_{66}^kh^kV_t'' & = 0 \\ \frac{a_6}{6h^k}V_b - \frac{a_7}{6h^k}V_t - \frac{a_8+6C_{33}^k}{6h^k}W_b - \frac{2a_8-6C_{33}^k}{6h^k}W_t - \frac{a_4}{6h^k}U_b' + \frac{a_3}{6h^k}U_t' - \frac{1}{6}C_{55}^kh^kW_b'' - \frac{1}{3}C_{55}^kh^kW_t'' & = 0 \end{cases} \quad (43)$$

where the prime or upper suffix ' denotes the ordinary derivative d/dx and

$$\begin{aligned} a_1^k &= h^{k^2}(\alpha_m^2 C_{66}^k - \omega^2 \rho_k) \quad , \quad a_2^k = \alpha_m h^{k^2}(C_{12}^k + C_{66}^k) \\ a_3^k &= 3h^k(C_{13}^k - C_{55}^k) \quad , \quad a_4^k = -3h^k(C_{13}^k + C_{55}^k) \\ a_5^k &= h^{k^2}(\omega^2 \rho_k - \alpha_m^2 C_{22}^k) \quad , \quad a_6^k = -3\alpha_m h^k(C_{23}^k + C_{44}^k) \\ a_7^k &= 3\alpha_m h^k(C_{23}^k - C_{44}^k) \quad , \quad a_8^k = 2h^{k^2}(\omega^2 \rho_k - \alpha_m^2 C_{44}^k) \end{aligned} \quad (44)$$

and the boundary conditions are

$$\begin{cases} F_{U_b}^k &= -\frac{1}{6}\alpha_m h^k C_{12}^k (2V_b^k + V_t^k) - \frac{1}{2}C_{13}^k (W_b^k - W_t^k) + \frac{1}{6}C_{11}^k h^k (2U_b'^k + U_t'^k) \\ F_{V_b}^k &= +\frac{1}{6}\alpha_m h^k C_{66}^k (2U_b^k + U_t^k) + \frac{1}{6}C_{66}^k h^k (2V_b'^k + V_t'^k) \\ F_{W_b}^k &= -\frac{1}{2}C_{55}^k (U_b^k - U_t^k) + \frac{1}{6}C_{55}^k h^k (2W_b'^k + W_t'^k) \\ F_{U_t}^k &= -\frac{1}{6}\alpha_m h^k C_{12}^k (V_b^k + 2V_t^k) - \frac{1}{2}C_{13}^k (W_b^k - W_t^k) + \frac{1}{6}C_{11}^k h^k (U_b'^k + 2U_t'^k) \\ F_{V_t}^k &= +\frac{1}{6}\alpha_m h^k C_{66}^k (U_b^k + 2U_t^k) + \frac{1}{6}C_{66}^k h^k (V_b'^k + 2V_t'^k) \\ F_{W_t}^k &= -\frac{1}{2}C_{55}^k (U_b^k - U_t^k) + \frac{1}{6}C_{55}^k h^k (W_b'^k + 2W_t'^k) \end{cases} \quad (45)$$

¹This is a necessary condition in order for the trigonometric function to be a solution of the differential equations and comply with the SS BCs

3. THE L-MATRIX METHOD

3.1. Use of the L matrix for systematic generation of the equations for N layers

The above equations are valid for only one layer. If more than one layer is used, the fundamental CUF nucleus \mathbf{K} (Eq. (18)) should be assembled across the new number of layers and the new equations of motion which will be coupled (layer by layer) should be developed all over again. For this reason a way of assembling directly the differential equations of motion and boundary conditions starting sequentially from layer 1 (Eqs. (43) and (45)) has been devised. This method hereafter is referred to as the L-matrix method. The method can find its applications in a multitude of problems where the number of differential equations to solve changes from one case to the other due to external factors (such as number of layers, order of the displacement models, etc...). It is inconvenient to rewrite the equations and solve the system for each case. This method uses a matrix \mathbf{L} to represent the system of differential equations. The matrix \mathbf{L} has a number of rows equal to the number of differential equations. In the present case, the number is 6 because $U_b^k = [U_b^k, V_b^k, W_b^k]$ and $U_t^k = [U_t^k, V_t^k, W_t^k]$. The number of columns is equal to the number of unknowns 6 in this case ($U_b^k = [U_b^k, V_b^k, W_b^k]$ and $U_t^k = [U_t^k, V_t^k, W_t^k]$) times the number of derivative orders which is 3, namely derivative 0, first order and second order for a total of 18 columns for 1 layer. The \mathbf{L} matrix can be split into 4 sub-matrices which will refer to the bottom layer, and top layer of each ply. e.g. the k^{th} ply.

The system for differential equation of Eq. (43) can thus be written in matrix

form as

$$\left[\begin{array}{c|c} \mathbf{L}_{BB}^k & \mathbf{L}_{BT}^k \\ \hline \mathbf{L}_{TB}^k & \mathbf{L}_{TT}^k \end{array} \right] \left[\begin{array}{c} \tilde{\mathbf{U}}_B^k \\ \tilde{\mathbf{U}}_T^k \end{array} \right] = \left[\begin{array}{c} \mathbf{0} \\ \mathbf{0} \end{array} \right] \quad (46)$$

where

$$\begin{aligned} \tilde{\mathbf{U}}_B^k &= [U_B^k, U_B^{l^k}, U_B^{ll^k}, V_B^k, V_B^{l^k}, V_B^{ll^k}, W_B^k, W_B^{l^k}, W_B^{ll^k}]^T \\ \tilde{\mathbf{U}}_T^k &= [U_T^k, U_T^{l^k}, U_T^{ll^k}, V_T^k, V_T^{l^k}, V_T^{ll^k}, W_T^k, W_T^{l^k}, W_T^{ll^k}]^T \end{aligned} \quad (47)$$

and

$$\mathbf{L}_{BB}^k = \begin{bmatrix} \frac{a_1^k + 3C_{55}^k}{3h^k} & 0 & -\frac{C_{11}^k h^k}{3} & 0 & \frac{a_2^k}{3h^k} & 0 & 0 & \frac{a_3^k}{6h^k} & 0 \\ 0 & -\frac{a_2^k}{3h^k} & 0 & -\frac{a_5^k - 3C_{44}^k}{3h^k} & 0 & -\frac{C_{66}^k h^k}{3} & \frac{a_7^k}{6h^k} & 0 & 0 \\ 0 & -\frac{a_3^k}{6h^k} & 0 & \frac{a_7^k}{6h^k} & 0 & 0 & -\frac{a_8^k - 3C_{33}^k}{3h^k} & 0 & -\frac{C_{55}^k h^k}{3} \end{bmatrix} \quad (48)$$

$$\mathbf{L}_{BT}^k = \begin{bmatrix} \frac{a_1^k - 6C_{55}^k}{6h^k} & 0 & -\frac{C_{11}^k h^k}{6} & 0 & \frac{a_2^k}{6h^k} & 0 & 0 & \frac{a_4^k}{6h^k} & 0 \\ 0 & -\frac{a_2^k}{6h^k} & 0 & -\frac{a_5^k + 6C_{44}^k}{6h^k} & 0 & -\frac{C_{66}^k h^k}{6} & \frac{a_6^k}{6h^k} & 0 & 0 \\ 0 & \frac{a_4^k}{6h^k} & 0 & -\frac{a_6^k}{6h^k} & 0 & 0 & -\frac{a_8^k + 6C_{33}^k}{6h^k} & 0 & -\frac{C_{55}^k h^k}{6} \end{bmatrix} \quad (49)$$

$$\mathbf{L}_{TB}^k = \begin{bmatrix} \frac{a_1^k - 6C_{55}^k}{6h^k} & 0 & -\frac{C_{11}^k h^k}{6} & 0 & \frac{a_2^k}{6h^k} & 0 & 0 & -\frac{a_4^k}{6h^k} & 0 \\ 0 & -\frac{a_2^k}{6h^k} & 0 & -\frac{a_5^k + 6C_{44}^k}{6h^k} & 0 & -\frac{C_{66}^k h^k}{6} & -\frac{a_6^k}{6h^k} & 0 & 0 \\ 0 & -\frac{a_4^k}{6h^k} & 0 & \frac{a_6^k}{6h^k} & 0 & 0 & -\frac{a_8^k + 6C_{33}^k}{6h^k} & 0 & -\frac{C_{55}^k h^k}{6} \end{bmatrix} \quad (50)$$

$$\mathbf{L}_{BB}^k = \begin{bmatrix} \frac{a_1^k + 3C_{55}^k}{3h^k} & 0 & -\frac{C_{11}^k h^k}{3} & 0 & \frac{a_2^k}{3h^k} & 0 & 0 & -\frac{a_3^k}{6h^k} & 0 \\ 0 & -\frac{a_2^k}{3h^k} & 0 & -\frac{a_5^k - 3C_{44}^k}{3h^k} & 0 & -\frac{C_{66}^k h^k}{3} & -\frac{a_7^k}{6h^k} & 0 & 0 \\ 0 & \frac{a_3^k}{6h^k} & 0 & -\frac{a_7^k}{6h^k} & 0 & 0 & -\frac{a_8^k - 3C_{33}^k}{3h^k} & 0 & -\frac{C_{55}^k h^k}{3} \end{bmatrix} \quad (51)$$

In this manner, the matrix \mathbf{L} can be assembled layer by layer just like a stiffness matrix assembly (see Figure (4) for details). Using \mathbf{L} , the system of differential equations can be written and subsequently solved for any number of layers in an automatic way.

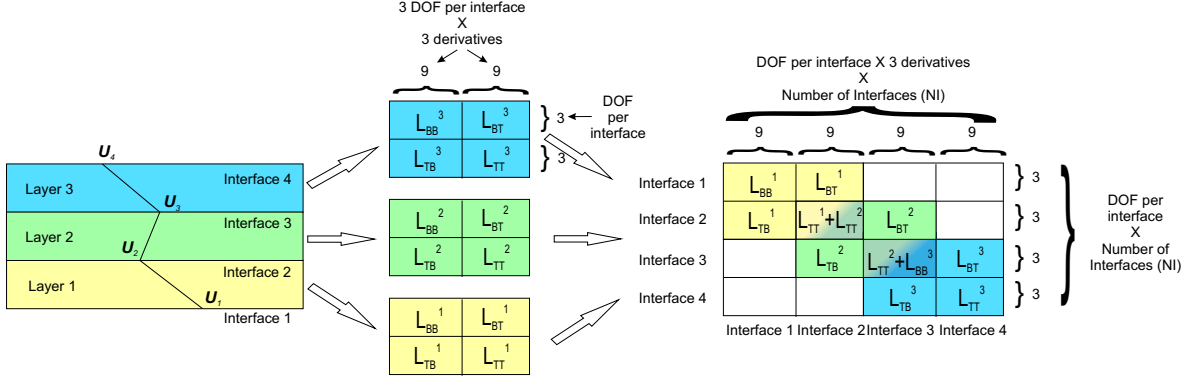


Figure 4: Schematic of how to assemble the L matrices for each layer to obtain the global L , i.e. the global system of differential equations

The global system of second order differential equations can be written then by using the global matrix L in the following form

$$\begin{bmatrix} L_{BB}^1 & L_{BT}^1 & 0 & \dots & 0 \\ L_{TB}^1 & L_{TT}^1 + L_{BB}^2 & L_{BT}^2 & \dots & 0 \\ 0 & L_{TB}^2 & L_{TT}^2 & \dots & 0 \\ \vdots & \vdots & \vdots & \ddots & \vdots \\ 0 & 0 & 0 & \dots & L_{TT}^{N_i} \end{bmatrix} \begin{bmatrix} \tilde{U}_1 \\ \tilde{U}_2 \\ \tilde{U}_3 \\ \vdots \\ \tilde{U}_{N_i} \end{bmatrix} = \begin{bmatrix} 0 \\ 0 \\ 0 \\ \vdots \\ 0 \end{bmatrix} \quad (52)$$

or,

$$L\tilde{U} = 0 \quad (53)$$

where the number of rows of the global L is equal to the number of unknown displacements per interface (DOF = 3, i.e. U^k, V^k, W^k) times the number of interfaces (NI), i.e. DOF \times NI and the number of columns is equal to the DOF \times NI \times 3 (number of derivatives, i.e. derivative 0, first and second).

The boundary conditions in Eq. (45) can also be written in matrix form as

$$\begin{bmatrix} \mathbf{F}_B^k \\ \mathbf{F}_T^k \end{bmatrix} = \begin{bmatrix} \mathbf{B}_{BB}^k & \mathbf{B}_{BT}^k \\ \mathbf{B}_{TB}^k & \mathbf{B}_{TT}^k \end{bmatrix} \begin{bmatrix} \hat{\mathbf{U}}_B^k \\ \hat{\mathbf{U}}_T^k \end{bmatrix} \quad (54)$$

where

$$\begin{aligned} \hat{\mathbf{U}}_B^k &= [U_B^k, U_B^{tk}, V_B^k, V_B^{tk}, W_B^k, W_B^{tk}]^T \\ \hat{\mathbf{U}}_T^k &= [U_T^k, U_T^{tk}, V_T^k, V_T^{tk}, W_T^k, W_T^{tk}]^T \end{aligned} \quad (55)$$

and

$$\mathbf{B}_{BB}^k = \begin{bmatrix} 0 & \frac{C_{11}^k h^k}{3} & -\frac{\alpha_m C_{12}^k h^k}{3} & 0 & -\frac{C_{13}^k h^k}{2} & 0 \\ \frac{\alpha_m C_{66}^k h^k}{3} & 0 & 0 & \frac{C_{66}^k h^k}{3} & 0 & 0 \\ -\frac{C_{55}^k h^k}{2} & 0 & 0 & 0 & 0 & \frac{C_{55}^k h^k}{3} \end{bmatrix} \quad (56)$$

$$\mathbf{B}_{BT}^k = \begin{bmatrix} 0 & \frac{C_{11}^k h^k}{6} & -\frac{\alpha_m C_{12}^k h^k}{6} & 0 & \frac{C_{13}^k h^k}{2} & 0 \\ \frac{\alpha_m C_{66}^k h^k}{6} & 0 & 0 & \frac{C_{66}^k h^k}{6} & 0 & 0 \\ \frac{C_{55}^k h^k}{2} & 0 & 0 & 0 & 0 & \frac{C_{55}^k h^k}{6} \end{bmatrix} \quad (57)$$

$$\mathbf{B}_{TB}^k = \begin{bmatrix} 0 & \frac{C_{11}^k h^k}{6} & -\frac{\alpha_m C_{12}^k h^k}{6} & 0 & -\frac{C_{13}^k h^k}{2} & 0 \\ \frac{\alpha_m C_{66}^k h^k}{6} & 0 & 0 & \frac{C_{66}^k h^k}{6} & 0 & 0 \\ -\frac{C_{55}^k h^k}{2} & 0 & 0 & 0 & 0 & \frac{C_{55}^k h^k}{6} \end{bmatrix} \quad (58)$$

$$\mathbf{B}_{TT}^k = \begin{bmatrix} 0 & \frac{C_{11}^k h^k}{3} & -\frac{\alpha_m C_{12}^k h^k}{3} & 0 & \frac{C_{13}^k h^k}{2} & 0 \\ \frac{\alpha_m C_{66}^k h^k}{3} & 0 & 0 & \frac{C_{66}^k h^k}{3} & 0 & 0 \\ \frac{C_{55}^k h^k}{2} & 0 & 0 & 0 & 0 & \frac{C_{55}^k h^k}{3} \end{bmatrix} \quad (59)$$

As before, the matrix \mathbf{B} can be assembled layer by layer as a normal stiffness matrix see Figure (5). Using \mathbf{B} , the equations of the boundary conditions can be written for any number of layers in an automatic form.

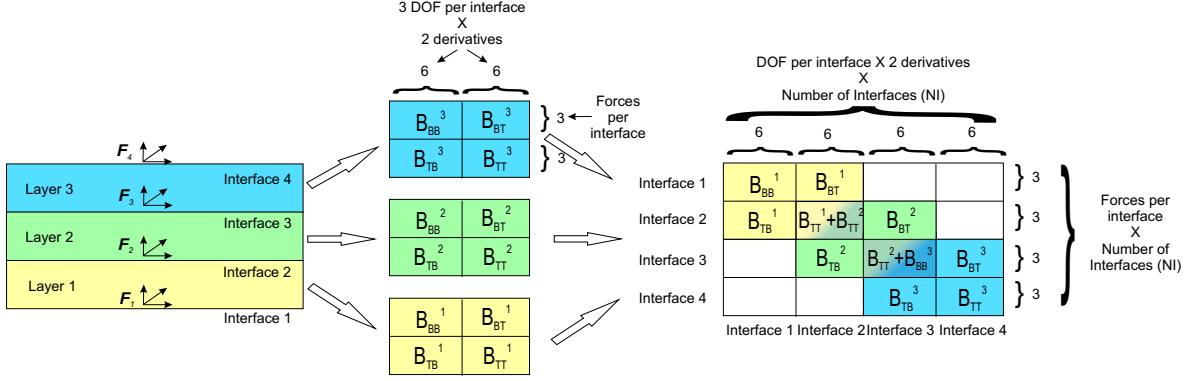


Figure 5: Schematic of how to assemble the B matrices for each layer to obtain the global B , i.e. the global equations of the boundary conditions

$$\begin{bmatrix} F_1 \\ F_2 \\ F_3 \\ \vdots \\ F_{NI} \end{bmatrix} = \begin{bmatrix} B_{BB}^1 & B_{BT}^1 & 0 & \dots & 0 \\ B_{TB}^1 & B_{TT}^1 + B_{BB}^2 & B_{BT}^2 & \dots & 0 \\ 0 & B_{TB}^2 & B_{TT}^2 & \dots & 0 \\ \vdots & \vdots & \vdots & \ddots & \vdots \\ 0 & 0 & 0 & \dots & B_{TT}^{NI} \end{bmatrix} \begin{bmatrix} \hat{U}_1 \\ \hat{U}_2 \\ \hat{U}_3 \\ \vdots \\ \hat{U}_{NI} \end{bmatrix} \quad (60)$$

or,

$$F = B\hat{U} \quad (61)$$

where rows of the global B are equal to the number of forces per interface which is equal to the number of displacements per interface (DOF = 3, i.e. F_U^k, F_V^k, F_W^k) times the number of interfaces ($NI=N_l + 1$), i.e. DOF \times NI and the number of columns is equal to the DOF \times NI \times 2 derivatives, i.e. derivative 0 and first.

3.2. Solution of the differential equations with the L matrix method

The procedure to solve a system of ordinary differential equation of the second order with constant coefficients is given in (APPENDIX B). Once the matrix $\tilde{\mathbf{S}}$ (see Eq. (B.3)) is known, the matrix \mathbf{S} (see Eq. (B.7)) can then be consequently obtained via a change of variables . As explained in (APPENDIX B) a change of variable to reduce the second order system to a first order system is sought in the following form:

$$\begin{aligned} \mathbf{Z} &= [Z_1, Z_2, \dots, Z_N]^T = \hat{\mathbf{U}} = \\ &= [U_1, U_1', V_1, V_1', W_1, W_1', U_2, U_2', V_2, V_2', W_2, W_2', \dots, V_{NI}, W_{NI}, W_{NI}']^T \end{aligned} \quad (62)$$

where $N = 3 \times NI \times 2$ is the dimension of the unknown vector as well as the number of differential equations.

The main task now is to find an algorithm to transform the assembled \mathbf{L} (Eq. (53)) matrix into the matrix $\tilde{\mathbf{S}}$. In fact, by looking at Eq. (B.2) it could be seen that only second derivatives should be on the left hand side (LHS) of the differential equations while, by looking at Eq. (43) for layer 1 and then looking at the system of equations written in compact form for N_l layers (see Eq. (53)). Thus for each equations more than one second derivative appears. In order to obtain the matrix \mathbf{S} from the global \mathbf{L} matrix decoupling between the second derivatives is necessary and should be done row by row and only one second derivative should appear in each row. In this context the matrix \mathbf{L} is devised so that every third column shows the value of the coefficient of a second derivative which makes decoupling of the second derivatives easier. In fact, in order to decouple the equations, these coefficients should be: (i) -1 for line 1 column 3 and zero for column 6, 9, \dots , N ; (ii) -1 for line 2 column 6 and zero for column 3, 9, \dots , N ; (iii) and so on till -1 for line N

column N and zero for column $3, 6, 9, \dots, N - 3$.

Once this is achieved, only one second derivative appears in each row and by setting the value of the coefficient to -1 , is equivalent to moving that term on the LHS of the equation so that if these columns are removed from the transformed \mathbf{L} , which is called $\hat{\mathbf{L}}$, only the right hand side of the equation is left, that is the matrix of the coefficient of the differential equations called $\tilde{\mathbf{S}}$ from which \mathbf{S} can be obtained by adding rows with 0's and 1's to include the change of variables (see (APPENDIX B), Eq. (B.3) and (B.7)). The algorithm to transform the \mathbf{L} to the $\tilde{\mathbf{S}}$ is named by the authors forward and backward partial Gauss elimination (FBPGE) and is explained in details in (APPENDIX C).

Once the matrix $\tilde{\mathbf{S}}$ (Eq. (B.3)) is obtained, and subsequently transformed to \mathbf{S} (B.7), by following the procedure (explained in detail in (APPENDIX B)) the solution can be written in matrix form as:

$$\begin{bmatrix} Z_1 \\ Z_2 \\ \vdots \\ Z_N \end{bmatrix} = \begin{bmatrix} \delta_{11} & \delta_{21} & \dots & \delta_{N1} \\ \delta_{12} & \delta_{22} & \dots & \delta_{N2} \\ \vdots & \vdots & \ddots & \vdots \\ \delta_{1N} & \delta_{2N} & \dots & \delta_{NN} \end{bmatrix} \begin{bmatrix} C_1 e^{\lambda_1 x} \\ C_2 e^{\lambda_2 x} \\ \vdots \\ C_N e^{\lambda_N x} \end{bmatrix} \quad (63)$$

where λ_i is the i^{th} eigenvalue of the \mathbf{S} matrix, δ_{ij} is the j^{th} element of the i^{th} eigenvector and C_i are the integration constants which needs to be determined by using the boundary conditions.

The above equation can be written in matrix form as:

$$\mathbf{Z} = \delta \mathbf{C} e^{\lambda x} \quad (64)$$

It should be recognised that the vector \mathbf{Z} does not only contain the displacements but also their first derivatives which will come at hand when

computing the boundary conditions. If only the displacements are needed, by remembering Eq. (62) only the rows 1, 3, 5, \dots , N should be taken, giving a solution in the following form:

$$\begin{aligned}
U_1(x) &= C_1\delta_{11}e^{\lambda_1x} + C_2\delta_{21}e^{\lambda_2x} + \dots + C_N\delta_{N1}e^{\lambda_Nx} \\
V_1(x) &= C_1\delta_{13}e^{\lambda_1x} + C_2\delta_{23}e^{\lambda_2x} + \dots + C_N\delta_{N3}e^{\lambda_Nx} \\
W_1(x) &= C_1\delta_{15}e^{\lambda_1x} + C_2\delta_{25}e^{\lambda_2x} + \dots + C_N\delta_{N5}e^{\lambda_Nx} \\
&\vdots \\
W_{NI}(x) &= C_1\delta_{1(N-1)}e^{\lambda_1x} + C_2\delta_{2(N-1)}e^{\lambda_2x} + \dots + C_N\delta_{N(N-1)}e^{\lambda_Nx}
\end{aligned} \tag{65}$$

Once the displacements and their first derivatives are known, the boundary conditions can be easily obtained by recalling that the global $\hat{\mathbf{U}}$ is equal to \mathbf{Z} (Eq. (62)) and by substituting the solution (Eq. (64)) into the boundary conditions (Eq. (61)). This leads to

$$\mathbf{F} = \mathbf{B}\delta\mathbf{C}e^{\lambda\mathbf{x}} = \mathbf{\Lambda}\mathbf{C}e^{\lambda\mathbf{x}} \tag{66}$$

where the matrix $\mathbf{\Lambda}$ contains the coefficients for the calculating the boundary conditions and has dimensions $(3 \text{ DOF} \times \text{NI}) \times (\text{N})$ where N is equal to $3 \text{ DOF} \times \text{NI} \times 2$ derivatives. The boundary conditions can be written in explicit form as

$$\begin{aligned}
F_{U_1}(x) &= C_1\Lambda_{11}e^{\lambda_1x} + C_2\Lambda_{12}e^{\lambda_2x} + \dots + C_N\Lambda_{1N}e^{\lambda_Nx} \\
F_{V_1}(x) &= C_1\Lambda_{21}e^{\lambda_1x} + C_2\Lambda_{22}e^{\lambda_2x} + \dots + C_N\Lambda_{2N}e^{\lambda_Nx} \\
F_{W_1}(x) &= C_1\Lambda_{31}e^{\lambda_1x} + C_2\Lambda_{32}e^{\lambda_2x} + \dots + C_N\Lambda_{3N}e^{\lambda_Nx} \\
&\vdots \\
F_{W_{NI}}(x) &= C_1\Lambda_{(N/2)1}e^{\lambda_1x} + C_2\Lambda_{(N/2)2}e^{\lambda_2x} + \dots + C_N\Lambda_{(N/2)N}e^{\lambda_Nx}
\end{aligned} \tag{67}$$

Although resorting to the L matrix seems extremely convoluted and complicated, it is in fact the simplest way to solve a problem of such complex nature. The matrix \mathbf{L} is simply a different way to write the differential equations for one layer. The greatest advantage is that it allows an automatic assembly of the differential equations for different layers (and if needed for different plate theories with increasing orders). In contrast to the structural problems in the literature, where by using a Navier type solution, the system becomes algebraic, or by using Levy's solution the equations are written for one configuration and then solved, by using \mathbf{L} matrix method the differential equations can be written automatically, thus allowing the solution of the problem for any number of layer in an automatic way. Earlier attempts to assemble directly the \mathbf{S} matrix instead of using the L -matrix method failed due to the fact that more than one second derivative appears in each equation and then decoupling on the second derivatives was needed. This decoupling, physically, represents the connection between each and every interface through the thickness and not only for the adjacent one but also for the subsequent ones. In fact, after decoupling of the second derivatives, unknowns coming from all the interfaces appear in each equation.

4. DYNAMIC STIFFNESS FORMULATION

4.1. *Dynamic stiffness matrix*

Once the boundary conditions and displacements are found in terms of the N integration constants, the classical method to solve the problem would be to put N displacements and/or forces to zero in order to simulate the boundary condition [4, 52, 53]. These would translate into following possible

scenarios (i) free boundary: forces equal zero at $x = 0$ and $x = b$; (ii) clamped boundary: displacements equal zero at $x = 0$ and $x = b$; (iii) simply supported: a combination of displacements and forces equal to zero at $x = 0$ and $x = b$. A limitation to the classical method is that it can only be applied to study simple individual plates. By contrast, the solution obtained thus far, can be used to obtain the dynamic stiffness matrix of an element (similar to spectral elements [54]) which can be assembled to obtain the closed form exact results for geometrically more complex structures.

The procedure to obtain the DS matrix for any structural element can be summarised as:

- (i) Seek a closed form solution of the governing differential equations of motion for a structural element in free vibration.
- (ii) Apply a number of general boundary conditions equal to twice the number of integration constants in algebraic form; these are usually nodal displacements and forces.
- (iii) Eliminate the constants by relating the harmonically varying nodal forces to the corresponding displacements which generates the frequency dependent dynamic stiffness matrix connecting the nodal forces to the nodal displacements.

The procedure to obtain closed form solution has already been explained in the previous section. This should now be followed by the imposition of generic boundary conditions on each interface for displacements and forces (see Fig. (6)).

Starting from the displacements boundary conditions (see Fig. (6)), we can

write:

At $x = 0$:

$$\begin{aligned}
U_1(0) &= -\overline{U1}_1, V_1(0) = -\overline{V1}_1, W_1(0) = -\overline{W1}_1 \\
U_2(0) &= -\overline{U1}_2, V_2(0) = -\overline{V1}_2, W_2(0) = -\overline{W1}_2 \\
&\vdots \\
U_{NI}(0) &= -\overline{U1}_{NI}, V_{NI}(0) = -\overline{V1}_{NI}, W_{NI}(0) = -\overline{W1}_{NI}
\end{aligned} \tag{68}$$

At $x = b$:

$$\begin{aligned}
U_1(b) &= \overline{U2}_1, V_1(b) = \overline{V2}_1, W_1(b) = \overline{W2}_1 \\
U_2(b) &= \overline{U2}_2, V_2(b) = \overline{V2}_2, W_2(b) = \overline{W2}_2 \\
&\vdots \\
U_{NI}(b) &= \overline{U2}_{NI}, V_{NI}(b) = \overline{V2}_{NI}, W_{NI}(b) = \overline{W2}_{NI}
\end{aligned} \tag{69}$$

By formulating Eqs. (65) for $x = 0$ and $x = b$ and applying the BC in Eqs. (68) and (69), the following matrix relation for the nodal displacements is obtained:

$$\begin{bmatrix} \overline{U1}_1 \\ \overline{V1}_1 \\ \overline{W1}_1 \\ \vdots \\ \overline{W1}_{NI} \\ \overline{U2}_1 \\ \overline{V2}_1 \\ \overline{W2}_1 \\ \vdots \\ \overline{W2}_{NI} \end{bmatrix} = \begin{bmatrix} -\delta_{11} & -\delta_{21} & \dots & -\delta_{N1} \\ -\delta_{13} & -\delta_{23} & \dots & -\delta_{N3} \\ -\delta_{15} & -\delta_{25} & \dots & -\delta_{N5} \\ \vdots & \vdots & \ddots & \vdots \\ -\delta_{1(N-1)} & -\delta_{2(N-1)} & \dots & -\delta_{N(N-1)} \\ \delta_{11}e^{\lambda_1 b} & \delta_{21}e^{\lambda_2 b} & \dots & \delta_{N1}e^{\lambda_N b} \\ \delta_{13}e^{\lambda_1 b} & \delta_{23}e^{\lambda_2 b} & \dots & \delta_{N3}e^{\lambda_N b} \\ \delta_{15}e^{\lambda_1 b} & \delta_{25}e^{\lambda_2 b} & \dots & \delta_{N5}e^{\lambda_N b} \\ \vdots & \vdots & \ddots & \vdots \\ \delta_{1(N-1)}e^{\lambda_1 b} & \delta_{2(N-1)}e^{\lambda_2 b} & \dots & \delta_{N(N-1)}e^{\lambda_N b} \end{bmatrix} \begin{bmatrix} C_1 \\ C_2 \\ C_3 \\ \vdots \\ C_{N/2} \\ C_{N/2+1} \\ C_{N/2+2} \\ C_{N/2+3} \\ \vdots \\ C_N \end{bmatrix} \tag{70}$$

The above equation can be written in more compact form as

$$\bar{\mathbf{U}} = \mathbf{AC} \quad (71)$$

Also for the forces, general nodal forces are used as boundary conditions (see Fig. (6)):

At $x = 0$:

$$\begin{aligned} F_{U_1}(0) &= -\bar{F1}_{U_1}, F_{V_1}(0) = -\bar{F1}_{V_1}, F_{W_1}(0) = -\bar{F1}_{W_1} \\ F_{U_2}(0) &= -\bar{F1}_{U_2}, F_{V_2}(0) = -\bar{F1}_{V_2}, F_{W_2}(0) = -\bar{F1}_{W_2} \\ &\vdots \\ F_{U_{NI}}(0) &= -\bar{F1}_{U_{NI}}, F_{V_{NI}}(0) = -\bar{F1}_{V_{NI}}, F_{W_{NI}}(0) = -\bar{F1}_{W_{NI}} \end{aligned} \quad (72)$$

At $x = b$:

$$\begin{aligned} F_{U_1}(b) &= \bar{F2}_{U_1}, F_{V_1}(b) = \bar{F2}_{V_1}, F_{W_1}(b) = \bar{F2}_{W_1} \\ F_{U_2}(b) &= \bar{F2}_{U_2}, F_{V_2}(b) = \bar{F2}_{V_2}, F_{W_2}(b) = \bar{F2}_{W_2} \\ &\vdots \\ F_{U_{NI}}(b) &= \bar{F2}_{U_{NI}}, F_{V_{NI}}(b) = \bar{F2}_{V_{NI}}, F_{W_{NI}}(b) = \bar{F2}_{W_{NI}} \end{aligned} \quad (73)$$

By calculating Eqs. (67) in $x = 0$ and $x = b$ and applying the BC in Eqs. (72) and (73), the following matrix relation for the nodal displacements is

obtained:

$$\begin{bmatrix} \overline{F1}_{U_1} \\ \overline{F1}_{V_1} \\ \overline{F1}_{W_1} \\ \vdots \\ \overline{F1}_{W_{Nl}} \\ \overline{F2}_{U_1} \\ \overline{F2}_{V_1} \\ \overline{F2}_{W_1} \\ \vdots \\ \overline{F2}_{W_{Nl}} \end{bmatrix} = \begin{bmatrix} -\Lambda_{11} & -\Lambda_{12} & \dots & -\Lambda_{1N} \\ -\Lambda_{21} & -\Lambda_{22} & \dots & -\Lambda_{2N} \\ -\Lambda_{31} & -\Lambda_{32} & \dots & -\Lambda_{3N} \\ \vdots & \vdots & \ddots & \vdots \\ -\Lambda_{(N/2)1} & -\Lambda_{(N/2)2} & \dots & -\Lambda_{(N/2)N} \\ \Lambda_{11}e^{\lambda_1 b} & \Lambda_{12}e^{\lambda_2 b} & \dots & \Lambda_{1N}e^{\lambda_N b} \\ \Lambda_{21}e^{\lambda_1 b} & \Lambda_{22}e^{\lambda_2 b} & \dots & \Lambda_{2N}e^{\lambda_N b} \\ \Lambda_{31}e^{\lambda_1 b} & \Lambda_{32}e^{\lambda_2 b} & \dots & \Lambda_{3N}e^{\lambda_N b} \\ \vdots & \vdots & \ddots & \vdots \\ \Lambda_{(N/2)1}e^{\lambda_1 b} & \Lambda_{(N/2)2}e^{\lambda_2 b} & \dots & \Lambda_{(N/2)N}e^{\lambda_N b} \end{bmatrix} \begin{bmatrix} C_1 \\ C_2 \\ C_3 \\ \vdots \\ C_{N/2} \\ C_{N/2+1} \\ C_{N/2+2} \\ C_{N/2+3} \\ \vdots \\ C_N \end{bmatrix} \quad (74)$$

The above equation can be written in more compact for as

$$\overline{F} = RC \quad (75)$$

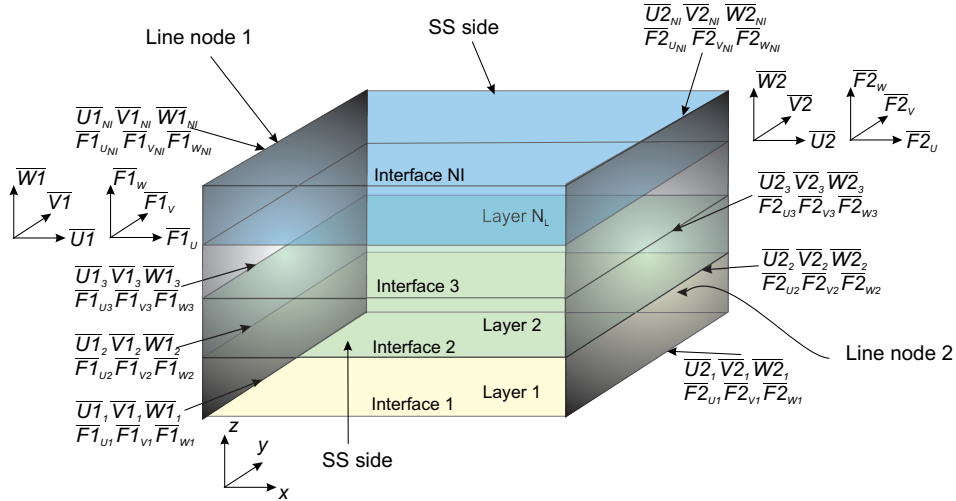


Figure 6: Edge conditions of the plate element and sign conventions

The constant vector \mathbf{C} from Eqs. (71) and (75) can now be eliminated to give the dynamic stiffness matrix of one element:

$$\overline{\mathbf{F}} = \mathbf{K}\overline{\mathbf{U}} \quad (76)$$

where

$$\mathbf{K} = \mathbf{R}\mathbf{A}^{-1} \quad (77)$$

4.2. Assembly of the DS elements

The dynamic stiffness matrix given by Eqs. (77) is the basic building block to compute the exact natural frequencies and mode shapes of a plate which is simply supported on at least two of their opposite sides and for such individual plate problems no coordinate transformation or offset connections are needed. As the DSM has many of the general features of the FEM, it has thus the capability to assemble element stiffness matrices to form the overall dynamic stiffness matrix of complex structures consisting of plate elements (see Figure (7)). For instance, plates with stringers connected at any arbitrary orientations can be analysed and yet exact results can be achieved.

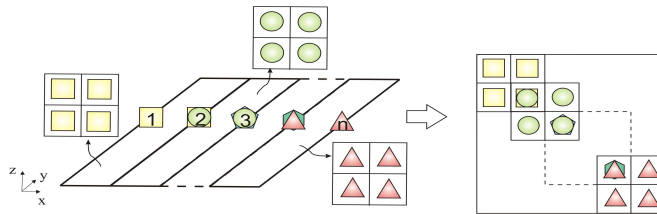


Figure 7: Assembly of dynamic stiffness matrices

The global dynamic stiffness matrix can be written as

$$\overline{\mathbf{F}}_G = \mathbf{K}_G\overline{\mathbf{U}}_G \quad (78)$$

where \mathbf{K}_G is a square matrix of dimensions: $\text{DOF} \times \text{NI} \times \text{NN}$ (total number of nodes in the structure).

4.3. Boundary conditions

The boundary conditions can be applied by using the well-known penalty method (often used in the FEM) or by simply removing rows and columns of the dynamic stiffness matrix corresponding to the degrees of freedom which need to be constrained. Due to the presence of degrees of freedom at each interface (see Figure (6)), a multitude of boundary condition can be applied at the required line nodes. A choice on whether or not to constrain the interface nodes at the boundaries has also to be addressed. As a matter of fact, layer wise plate models allow for constrains to be applied through the thickness differently from classical plate theories, having a quasi-3D representation. Although there are multiple possibilities, the implemented constrain types the associated degrees of freedom that are penalised are:

- Free end (F): no penalty
- Clamped end (C): penalty applied to U^k , V^k , W^k at each and every interface
- Simply supported (S): penalty applied to V^k , W^k at each and every interface thought the thickness

4.4. The Wittrick-Williams algorithm

For free vibration analysis of structures, the FEM generally leads to a linear eigenvalue problem. By contrast, the DSM leads to a transcendental (non-linear) eigenvalue problem for which the Wittrick-Williams algorithm

[55] is recognisably the best available solution technique at present.

The algorithm can be briefly summarised in the following steps:

- (i) A trial frequency ω^* is chosen to compute the dynamic stiffness matrix K^* of the final structure;
- (ii) K^* is reduced to its upper triangular form by Gauss elimination to obtain $K^{*\Delta}$ and the number of negative terms on the leading diagonal of $K^{*\Delta}$ is counted; this is known as the sign count $s(K^*)$ of the triangulated matrix;
- (iii) The number (j) of natural frequencies (ω) of the structure which lie below the trial frequency (ω^*) is then given by:

$$j = j_0 + s(K^*) \tag{79}$$

where j_0 is the number of natural frequencies of all individual elements with clamped-clamped (C-C) boundary conditions on their opposite sides which still lie below the trial frequency ω^* .

Assuming that j_0 is known, and $s(K^*)$ can be obtained by counting the number of negative terms in the diagonal of $K^{*\Delta}$, a suitable procedure can be devised, for example the bi-section method, to bracket any natural frequency between an upper and lower bound of the trial frequency ω^* to any desired accuracy.

However, the computation of j_0 can be cumbersome and may require additional sub-analysis to compute the C-C frequencies of the single elements composing the structure. For this reason the algorithm has been modified to avoid the computation of j_0 . The procedure involves computing the first

C-C frequency of the largest element in the global structure by running a sub-analysis. The largest element has also the lower C-C frequency of the whole structure. This frequency can be called omega limit ω_L^* and its limits the trial omega for which $j_0 = 0$. Thus, if the trial omega exceeds the omega limit, the structure is split automatically into smaller elements, for which, the new omega limit will be higher, and in this way additional frequencies can be computed.

4.5. Mode shape computation

Once natural frequencies have been computed, by using the global dynamic stiffness matrix of Eq. (78) and a random force vector \mathbf{F}_G , the nodal displacements corresponding to the given natural frequencies can be computed. So far, in the literature, the nodal displacements $\bar{\mathbf{U}}_G$ are used to plot the mode shapes [24–39, 43–46]. In order to have a detailed plot, a large number of elements is required. In fact, this is not necessary in DSM. A new procedure to obtain the modal displacement as a function of x, y, z has been devised and can be summarised in the following steps.

- (i) The global nodal displacement $\bar{\mathbf{U}}_G$ is split into the element by element displacement vector to give $\bar{\mathbf{U}}$. A cycle on the elements will be needed. The i^{th} element is analysed in the following steps.
- (ii) By using the nodal displacements $\bar{\mathbf{U}}$ the integration constants \mathbf{C} of the element can be computed by using Eq. (71).
- (iii) By using Eq. (65), the unknown displacements can be computed as a function of x .
- (iv) By using Eq. (42), the unknown displacements can be computed as a function of x, y and the time t (if an animated plot is needed).

- (v) By using Eqs. (26) and (27) the 3D plot of the required mode and required element can be visualised.

By following the above procedure, with only 1 element, the exact mode shapes can be obtained.

5. SUMMARY OF THE DSM FORMULATION FOR A LAYER WISE MODEL

Due to the complicated and convoluted steps required for developing this advanced dynamic stiffness element, a summary of the required steps is presented below.

- (i) Calculate the \mathbf{L} (Eq. (46)) and \mathbf{B} (Eq. (54)) matrices for each layer
- (ii) Assemble the \mathbf{L} matrix and \mathbf{B} matrix across the thickness layer by layer as explained in Figure (4) and (5) and Eqs. (52) and (60)
- (iii) Apply FBPGE (see (APPENDIX C)) to obtain the matrix $\tilde{\mathbf{S}}$ and then transform it to reduce the order (see (APPENDIX B)) to obtain \mathbf{S} (Eq. (B.7))
- (iv) Solve the reduced order system of differential equations to obtain the displacements and boundary conditions (integration constants are still unknown), i.e. calculate $\boldsymbol{\delta}$ and λ to find the displacements (Eq. (64)) and $\mathbf{\Lambda}$ to find the boundary conditions (Eq. (66))
- (v) Calculate the matrix \mathbf{A} (Eq. (70)) for the displacements and the matrix \mathbf{R} (Eq. (74)) for the forces
- (vi) Calculate the DS matrix of the single multilayered element as $\mathbf{K} = \mathbf{A}^{-1}\mathbf{R}$

- (vii) Once the DS matrix of the single element is obtained, it is then possible to rotate and assemble the elements to study complex structures (section (4.2))
- (viii) Apply the required boundary conditions to the global structure (section (4.3))
- (ix) Solve the matrix by using the classical Wittrick and Williams algorithm (section (4.4)) to calculate the natural frequencies
- (x) Compute the mode shapes (section (4.5))

By following the above procedure, closed form analytical results for structures which can be modelled as strip assemblies can be obtained by conducting a layer-wise analysis which increases the accuracy of result very considerably. The proposed method allows the investigation of sandwich plates with various interfaces, and can be used for modelling even delamination which is indeed a very difficult problem.

6. RESULTS

The layer wise dynamic stiffness elements developed above, have been validated, assessed and used to obtain a number of benchmark solutions. The plate geometry, material properties and stacking sequences used in this paper are those used by Noor et al. [56] to obtain the closed form 3D analytical solutions for simply supported square plates. The same plate parameters have been used by Carrera [57] when assessing a large number of plate theories based on the CUF. The closed form results available in the literature are obtained by using a Navier type solution, thus they are valid only for plates which are simply supported on its four edges.

The plate studied has a side over thickness ratio a/h of 5 and has a square geometry. The material properties are as follow: $G_{12}/E_2 = G_{13}/E_2 = 0.5$, $G_{23}/E_2 = 0.35$, $\nu_{12} = \nu_{13} = 0.3$, $\nu_{23} = 0.49$. Four different staking sequences are investigated: two skew-symmetric $[0/90]$ and $[0/90]_5$ and two symmetric $[0/90/90/0]$ and $[0/90/0/90/\bar{0}]_S$. The total thickness of the 0 degree layers is equal to the total thickness of the 90 degree layers for all the configurations. Furthermore, 2 stiffness ratios are used, namely $E_1/E_2 = 3$ and $E_1/E_2 = 30$. The frequencies are given in non-dimensional form as $\omega^* = \omega h \sqrt{\rho/E_2}$.

6.1. Validation and assessment for simply supported plates

Tables (1) and (2) show the results obtained for a plate simply supported on all its four sides (SSSS) by using the new dynamic stiffness element (DySAP LD1). They are compared with Navier type solutions based on different plate theories such has CUF LD1, CUF ED1d $\chi=5/6$, and CUF ED1d $\chi=\infty$. In the table, LD1 refers to a first order layer wise theory which is equivalent to the one implemented in the paper, ED1d $\chi=5/6$ refers to a first order equivalent single layer theory with a shear correction factor of $\chi = 5/6$, and ED1d $\chi=\infty$ is the equivalent of a classical lamination theory CLT [57]. It can be seen that the results based on a layer wise theory of the first order (LD1) obtained here by DySAP and by a Navier type solution (CUF LD1) by Carrera [57] are in exact agreement. The results are also compared with the exact 3D solution obtained by Noor et al. [56]. It can be seen that the error incurred by the LD1 theory is consistently lower than that made by equivalent single layers theories ED1 (such as CLT). It should also be noted that LD1 shows a larger error when the single ply of the laminate have a larger thickness ratio (such as for the $[0/90]$). This shows that, different

from isotropic plates where the total thickness compared to the side length would define if a plate is “thin” or “thick”, for composite plates, the thickness of the single ply is more important than the total thickness of the plate. For thicker plies, higher order theories should be used not to compromise the accuracy of results. Furthermore, the level of anisotropy, which can be defined by the stiffness ratio E_1/E_2 , also influences the accuracy of the results. Plates with higher stiffness ratio should be studied with more advanced theories.

Table 1: Fundamental dimensionless bending frequencies $\omega^* = \omega h \sqrt{\rho/E_2}$ for a square SSSS plate with 2 different skew-symmetric stacking sequences and stiffness ratio. Comparison of different theories with the 3D exact results and percentage error.

Lay-up	0/90				[0/90] ₅			
	3		30		3		30	
E_1/E_2	ω^*	%	ω^*	%	ω^*	%	ω^*	%
Exact 3D [56]	0.2392		0.3117		0.2530		0.4027	
DySAP LD1	0.2478	3.6	0.3210	3.0	0.2534	0.2	0.4042	0.4
CUF LD1 [57]	0.2478	3.6	0.3210	3.0	0.2534	0.2	0.4042	0.4
CUF ED1d $\chi=5/6$ [57]	0.261	9.1	0.3264	4.7	0.2723	7.6	0.4118	2.3
CUF ED1d $\chi=\infty$ [57]	0.2972	24.2	0.4066	30.4	0.3150	24.5	0.6435	59.8

Table 2: Fundamental dimensionless bending frequencies $\omega^* = \omega h \sqrt{\rho/E_2}$ for a square SSSS plate with 2 different symmetric stacking sequences and stiffness ratio. Comparison of different theories with the 3D exact results and percentage error.

Lay-up	0/90/90/0				[0/90/0/90/0] _S			
E_1/E_2	3		30		3		30	
Formulation	ω^*	%	ω^*	%	ω^*	%	ω^*	%
Exact 3D [56]	0.2516		0.3739		0.2535		0.4040	
DySAP LD1	0.2556	1.6	0.3808	1.8	0.2540	0.2	0.4058	0.4
CUF LD1 [57]	0.2556	1.6	0.3808	1.8	0.2540	0.2	0.4058	0.4
CUF ED1d $\chi=5/6$ [57]	0.2717	8.0	0.3871	3.5	0.2726	7.5	0.4118	1.9
CUF ED1d $\chi=\infty$ [57]	0.3157	25.5	0.6519	74.4	0.3157	24.5	0.6519	61.4

In order to improve the accuracy even further, more than one layer of LD1 element can be used within the same ply, i.e. a number of fictitious interfaces can be placed within the same physical ply to allow for a spline displacement distribution. Thus, LD1-1 means that one LD1 element is used through the thickness for each single ply of material (i.e. one straight displacement line for each ply), LD1-2 means that two elements have been used through the thickness of each single ply of material (i.e. a 2 line spline is used to describe the displacement within each layers) and so on. In Tables (3) and (4) the convergence of the layer wise theory to the exact 3D solution can be observed. The number of degree of freedom (DOF) used for each theory is also reported. Two dynamic stiffness elements have been used in the plane of the plate, while for LD1-1 only one layer for each ply through the thickness, i.e. 3 interfaces are employed. The number of DOF is computed by considering 3 DOF per interface (u, v, w) times the number of interfaces through the thickness, times the number of nodes of the plate elements. For

instance, for LD1-4, 3 DOF times 9 interfaces, times 3 nodes (2 elements) gives 81 DOF.

It can be observed that a lower number of fictitious interfaces are needed to obtain results close to the 3D exact solution for thin plies. This confirms that the important parameter when deciding how to model a composite plate is the thickness ratio of the single plies rather than the thickness ratio of the whole plate. Thicker plies and higher stiffness ratios require more interfaces, i.e. higher order theories.

Table 3: Fundamental dimensionless bending frequencies $\omega^* = \omega h \sqrt{\rho/E_2}$ and percentage error for a square SSSS plate with 2 different skew-symmetric stacking sequences and stiffness ratio. Convergence of the LD theory to the 3D exact solution by increasing the number of interfaces.

Lay-up	0/90					[0/90] ₅				
E_1/E_2	3		30			3		30		
Formulation	DOF	ω^*	%	ω^*	%	DOF	ω^*	%	ω^*	%
Exact 3D [56]		0.2392		0.3117			0.2530		0.4027	
DySAP LD1-1	27	0.2478	3.6	0.3210	3.0	99	0.2534	0.2	0.4042	0.4
DySAP LD1-2	45	0.2398	0.3	0.3169	1.7	189	0.2531	0.0	0.4031	0.1
DySAP LD1-4	81	0.2398	0.3	0.3135	0.6	369	0.2531	0.0	0.4028	0.0

Table 4: Fundamental dimensionless bending frequencies $\omega^* = \omega h \sqrt{\rho/E_2}$ and percentage error for a square SSSS plate with 2 different symmetric stacking sequences and stiffness ratio. Convergence of the LD theory to the 3D exact solution by increasing the number of interfaces.

Lay-up	0/90/90/0					[0/90/0/90/0] _S				
E_1/E_2	3		30			3		30		
Formulation	DOF	ω^*	%	ω^*	%	DOF	ω^*	%	ω^*	%
Exact 3D [56]		0.2516		0.3739			0.2535		0.4040	
DySAP LD1-1	45	0.2556	1.6	0.3808	1.8	90	0.2540	0.2	0.4058	0.4
DySAP LD1-2	81	0.2522	0.2	0.3758	0.5	171	0.2536	0.0	0.4045	0.1
DySAP LD1-4	153	0.2517	0.1	0.3744	0.1	333	0.2535	0.0	0.4041	0.0

The accuracy and efficiency of the finite element method is compared with the novel layer wise DS element implemented in DySAP. These are shown in Table (5) for the fundamental natural frequency. The two layer skew-symmetric [0/90] square plate with $a/h = 5$ and $E_1/E_2 = 30$ used previously is further examined. Both 3D and 2D finite element models have been constructed. The 3D models make use of 8-node brick elements (CHEXA) and are solved using NASTRAN. Two different meshes are used. A “coarse” mesh which uses 2 elements per ply where each element is a regular cube of dimension $a/20$. The total number of DOF is 13230. The “fine” mesh uses 10 elements per ply and a regular mesh of dimension $a/100$ which gives a total of 1285326 DOF. The 2D FE model uses 4-node laminate elements (CQUAD) and a fine regular mesh with a dimension of $a/50$. The total number of DOF for this mesh is 15606. A Ritz solution based on LD1 theory obtained by following the procedure in [58] is reported and makes use of 1296 DOF. Ritz solutions show a better spectral convergence when compared with FEM but

it is still an approximate method and requires a rather large number of DOF. DySAP LD1 on the other hand, with only 45 DOF, gives a closed form solution, thus no loss of accuracy at higher frequencies. Furthermore, the DySAP LD1-8 model with 8 fictitious interfaces for each ply, i.e. a total of 153 DOF, show the same accuracy of the 3D FEM model with a fine mesh which has 4 order of magnitude more DOF (see Table (5)). It should also be observed that the 2D FE model show a relatively good accuracy for such a thick plate. This is surprising because the theory used in the 2D FE model should be an equivalent single layer (ESL) first order shear deformation theory (FSDT), equivalent to the one called CUF ED1d $\chi=5/6$ in Table (1), which gives an error of 4.7% when compared with the results using 3D theory. The use of FSDT for composites raises some concerns about the shear correction factor χ to be used. By changing that shear correction factor, the results can be changed rather significantly. For this plate material and stacking sequence it seems that the 2D results give a small error, but for other laminates, the error could be much higher [18–20, 57]. Layer wise theory (as well as high order ESL) do not need any shear correction factor and thus can be considered much more reliable.

In Table (6), the same comparison is made for the first 10 natural frequencies. No 3D exact solution is available for higher frequencies thus the 3D fine mesh FE results are used for comparative purposes. It can be observed that DySAP LD1-8 shows a maximum error of 0.1 for all the frequencies with 153 DOF while, 2D FE result error increases for higher frequencies with a maximum error of 5% with 15606 DOF.

It should also be noted that the inplane modes called $m = 0$ by the authors

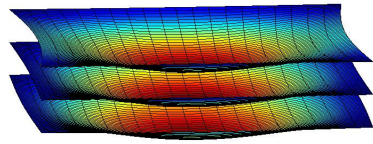
in [44] (which have been quite often, if not always overlooked during previous studies in the literature) have not been implemented in DySAP for the presented LD1 element. These modes are indicated with a * in the tables. More details on these particular frequencies and mode shapes can be found in [44]. Some characteristic and representative mode shapes have been shown in Figure (8) where they are compared against the ones obtained by 3D FE models. For the DySAP mode shapes, only the interfaces are plotted. It can be seen that the mode shapes are in excellent agreement.

Table 5: Fundamental frequency $\omega^* = \omega h \sqrt{\rho/E_2}$ and percentage error for a SSSS square plate: $0/90$ $E_1/E_2 = 30$. Comparison between the FEM, Ritz and the Dynamic Stiffness method.

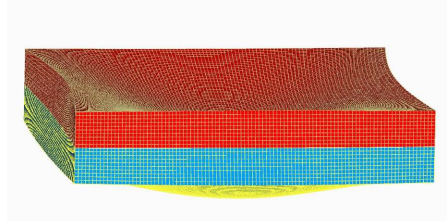
Theory	Exact 3D [56]	FEM 3D fine	FEM coarse	FEM 2D	DySAP LD1-8	DySAP LD1	Ritz LD1 [58]
DOF		1285326	13230	15606	153	45	1296
ω^*	0.3117	0.3120	0.3159	0.3088	0.3122	0.3210	0.3210
error%	/	0.1	1.3	-0.9	0.2	2.9	2.9

Table 6: First 10 frequencies $\omega^* = \omega h \sqrt{\rho/E_2}$ and percentage error for a SSSS square plate: $0/90$ $E_1/E_2 = 30$. Comparison between the FEM and the dynamic stiffness method.

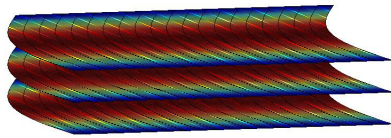
Theory	FEM 3D fine	FEM 3D coarse		FEM 2D		Ritz LD1 [58]		DySAP LD1-1		DySAP LD1-8	
DOF	1285326	13230		15606		1296		27		153	
Mode	ω^*	ω^*	%	ω^*	%	ω^*	%	ω^*	%	ω^*	%
1	0.3120	0.3159	1.2	0.3088	-1.0	0.3210	2.9	0.3210	2.9	0.3122	0.1
2	0.4443	0.4438	-0.1	0.4442	0.0	0.4443	0.0	0.4443	0.0	0.4443	0.0
3*	0.4443	0.4438	-0.1	0.4442	0.0	0.4443	0.0	/	/	/	/
4	0.6369	0.6480	1.7	0.6200	-2.6	0.6618	3.9	0.6618	3.9	0.6376	0.1
5	0.6370	0.6481	1.7	0.6200	-2.7	0.6618	3.9	0.6618	3.9	0.6376	0.1
6	0.8540	0.8624	1.0	0.8213	-3.8	0.8860	3.7	0.8860	3.7	0.8552	0.1
7	0.8884	0.8849	-0.4	0.8880	0.0	0.8886	0.0	0.8886	0.0	0.8886	0.0
8*	0.8884	0.8849	-0.4	0.8880	0.0	0.8886	0.0	/	/	/	/
9	1.0197	1.0323	1.2	0.9687	-5.0	1.0637	4.3	1.0637	4.3	1.0212	0.1
10	1.0198	1.0325	1.2	0.9687	-5.0	1.0637	4.3	1.0637	4.3	1.0212	0.1



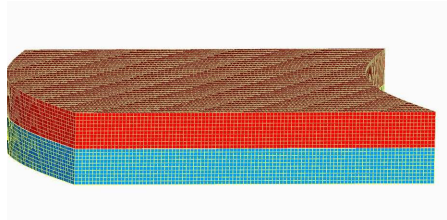
(a)



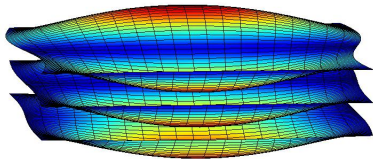
(b)



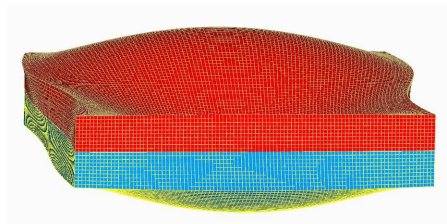
(c)



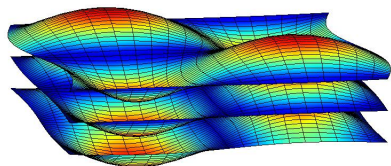
(d)



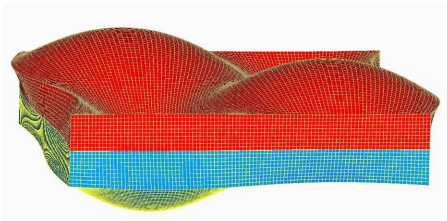
(e)



(f)



(g)



(h)

Figure 8: Comparison of some representative mode shapes obtained by DySAP or FEM (NASTRAN) for a SSSS plate. (a) DySAP mode 1, (b) FEM mode 1, (c) DySAP mode 2, (d) FEM mode 2, (e) DySAP mode 4, (f) FEM mode 4, (g) DySAP mode 6, (h) FEM mode 6.

6.2. Benchmark solutions for different boundary conditions

The plate studied in the previous section with SSSS boundary conditions is further examined with different boundary conditions such as SCSC, SSSC,SCSF,SSSF,SFSF (note that the dynamic stiffness method solutions can only be obtained when at least two opposite sides are simply supported). The results are reported in Tables (7)-(11). The DySAP LD1-8 solution is taken as benchmark results as it showed to be the most accurate one in the previous section (3D exact solution cannot be obtained for these boundary condition because a closed form solution of the 3D equation of motion with general conditions cannot be found in the literature). It can be seen that the error incurred by the 3D FEM is consistently below 2% for any of the chosen boundary conditions. On the other hand, the 2D FE error depends on the chosen boundary conditions. The largest error is for the clamped-clamped boundary. The superiority of the layer wise dynamic stiffness element in DySAP, particularly in terms of computationally efficiency can be seen by the number of degree of freedom needed to ascertain the benchmark solution. In Figure (9), three representative modes can be seen for the SFSF composite plate. Mode 3 and mode 9 show an “inplane” mode. Due to the skew symmetric lay-up the in-plane mode is coupled with out of plane one. For illustration, Mode 5 has been chosen because it clearly shows at the two free boundaries the change in slope of the displacements at the middle interface. The modes have been compared with the ones obtained by the FEM and they are in excellent agreement.

Table 7: First 10 frequencies $\omega^* = \omega h \sqrt{\rho/E_2}$ and percentage error for a SCSC square plate: 0/90 $E_1/E_2 = 30$. Benchmark solution and comparison with the FEM.

Theory	DySAP LD1-8	FEM 3D coarse		FEM 2D		Ritz LD1 [58]		DySAP LD-1	
DOF	153	13230		15606		1296		27	
Mode	ω^*	ω^*	%	ω^*	%	ω^*	%	ω^*	%
1	0.3830	0.3903	1.9	0.3676	-4.0	0.3967	3.6	0.3967	3.6
2*	/	0.4438	/	0.4442	/	0.4443	/	/	/
3	0.6706	0.6826	1.8	0.6457	-3.7	0.6967	3.9	0.6967	3.9
4	0.6908	0.7007	1.4	0.6480	-6.2	0.7163	3.7	0.7163	3.7
5	0.8924	0.8849	-0.8	0.8417	-5.7	0.9242	3.6	0.9242	3.6
6*	/	0.8994	/	0.8880	/	0.8860	/	/	/
7	1.0400	1.0522	1.2	0.9816	-5.6	1.0838	4.2	1.0838	4.2
8	1.0592	1.0685	0.9	0.9818	-7.3	1.0997	3.8	1.0997	3.8
9	1.2005	1.2015	0.1	1.1187	-6.8	1.2451	3.7	1.2451	3.7
10	1.2061	1.2058	0.0	1.1216	-7.0	1.2483	3.5	1.2483	3.5

Table 8: First 10 frequencies $\omega^* = \omega h \sqrt{\rho/E_2}$ and percentage error for a SSSC square plate: 0/90 $E_1/E_2 = 30$. Benchmark solution and comparison with the FEM.

Theory	DySAP LD1-8	FEM 3D coarse		FEM 2D		Ritz LD1 [58]		DySAP LD1-1	
DOF	153	13230		15606		1296		27	
Mode	ω^*	ω^*	%	ω^*	%	ω^*	%	ω^*	%
1	0.3456	0.3512	1.6	0.3371	-2.5	0.3568	3.2	0.3568	3.2
2*	/	0.4438	/	0.4442	/	0.4443	/	/	/
3	0.6527	0.6638	1.7	0.6321	-3.2	0.6778	3.8	0.6778	3.8
4	0.6659	0.6763	1.6	0.6354	-4.6	0.6910	3.8	0.6910	3.8
5	0.8746	0.8819	0.8	0.8322	-4.9	0.9061	3.6	0.9061	3.6
6*	/	0.8849	/	0.8880	/	0.8886	/	/	/
7	1.0298	1.0414	1.1	0.9748	-5.3	1.0729	4.2	1.0728	4.2
8	1.0394	1.0496	1.0	0.9749	-6.2	1.0808	4.0	1.0808	4.0
9	1.1605	1.1618	0.1	1.1129	-4.1	1.1979	3.2	1.1979	3.2
10	1.1881	1.1892	0.1	1.1148	-6.2	1.2323	3.7	1.2323	3.7

Table 9: First 10 frequencies $\omega^* = \omega h \sqrt{\rho/E_2}$ and percentage error for a SCSF square plate: 0/90 $E_1/E_2 = 30$. Benchmark solution and comparison with the FEM.

Theory	DySAP LD1-8	FEM 3D coarse		FEM 2D		Ritz LD1 [58]		DySAP LD1-1	
DOF	153	13230		15606		1296		27	
Mode	ω^*	ω^*	%	ω^*	%	ω^*	%	ω^*	%
1*	/	0.2221	/	0.2221	/	0.2221		/	/
2	0.2336	0.2369	1.4	0.2318	-0.8	0.2393	2.4	0.2393	2.4
3	0.4313	0.4360	1.1	0.4222	-2.1	0.4445	3.1	0.4445	3.1
4	0.5964	0.6092	2.2	0.5810	-2.6	0.6200	4.0	0.6200	4.0
5*	/	0.6649	/	0.6662	/	0.6664		/	/
6	0.7153	0.7227	1.0	0.6929	-3.1	0.7400	3.4	0.7400	3.4
7	0.7813	0.7890	1.0	0.7577	-3.0	0.8103	3.7	0.8103	3.7
8	0.9766	0.9786	0.2	0.9357	-4.2	1.0096	3.4	1.0096	3.4
9	0.9927	1.0077	1.5	0.9415	-5.2	1.0360	4.4	1.0360	4.4
10	1.0779	1.0838	0.5	1.0219	-5.2	1.1107	3.0	1.1194	3.8

Table 10: First 10 frequencies $\omega^* = \omega h \sqrt{\rho/E_2}$ and percentage error for a SSSF square plate: 0/90 $E_1/E_2 = 30$. Benchmark solution and comparison with the FEM.

Theory	DySAP LD1-8	FEM 3D coarse		FEM 2D			
DOF	153	13230		15606			
Mode	ω^*	ω^*	%	ω^*	%		
1	0.2077	0.2113	1.8	0.2071	-0.3	0.2133	2.7
2	0.2446	0.2467	0.9	0.2438	-0.3	0.2498	2.2
3	0.4123	0.4131	0.2	0.4128	0.1	0.4146	0.6
4*	/	0.4438	/	0.4442	/	/	/
5	0.5144	0.5166	0.4	0.5190	0.9	0.5280	2.6
6	0.5825	0.5963	2.4	0.5681	-2.5	0.6065	4.1
7	0.6140	0.6241	1.7	0.5997	-2.3	0.6365	3.7
8	0.7816	0.7840	0.3	0.7645	-2.2	0.8052	3.0
9	0.8458	0.8460	0.0	0.8510	0.6	0.8510	0.6
10	0.8769	0.8812	0.5	0.8802	0.4	0.9120	4.0

Table 11: First 10 frequencies $\omega^* = \omega h \sqrt{\rho/E_2}$ and percentage error for a SFSF square plate: $0/90$ $E_1/E_2 = 30$. Benchmark solution and comparison with the FEM.

Theory	DySAP LD1-8	FEM 3D coarse		FEM 2D		DySAP LD1-1	
DOF	153	13230		15606		27	
Mode	ω^*	ω^*	%	ω^*	%	ω^*	%
1	0.2183	0.2215	1.5	0.2174	-0.4	0.2239	2.5
2*	/	0.2221	/	0.2221	/	/	/
3	0.3998	0.4028	0.7	0.3992	-0.1	0.4085	2.2
4	0.4322	0.4328	0.1	0.4313	-0.2	0.4355	0.8
5	0.5909	0.6037	2.2	0.5763	-2.5	0.6145	4.0
6*	/	0.6649	/	0.6662	/	/	/
7	0.6996	0.7064	1.0	0.6812	-2.6	0.7232	3.4
8	0.7572	0.7654	1.1	0.7463	-1.4	0.7860	3.8
9	0.8669	0.8653	-0.2	0.8689	0.2	0.8699	0.4
10	0.9607	0.9627	0.2	0.9283	-3.4	0.9936	3.4

7. CONCLUSION

The dynamic stiffness method has been developed for a composite plate based on a first order layer wise formulation. The Carrera's Unified Formulation (CUF) has been used to obtain the equations of motions. A method has been devised to write the equation of motions of a single layer so that they can be assembled automatically for any number of layers . The method has been called the **L** matrix method. This method can find its application in any problem for which the number of equations to solve depends on external parameters (such the number of layers or the order of the formulation). An automatic method to solve the differential equations represented by the assembled *L* matrix has also been devised and eventually the dynamic stiffness method is developed. The dynamic stiffness element matrix

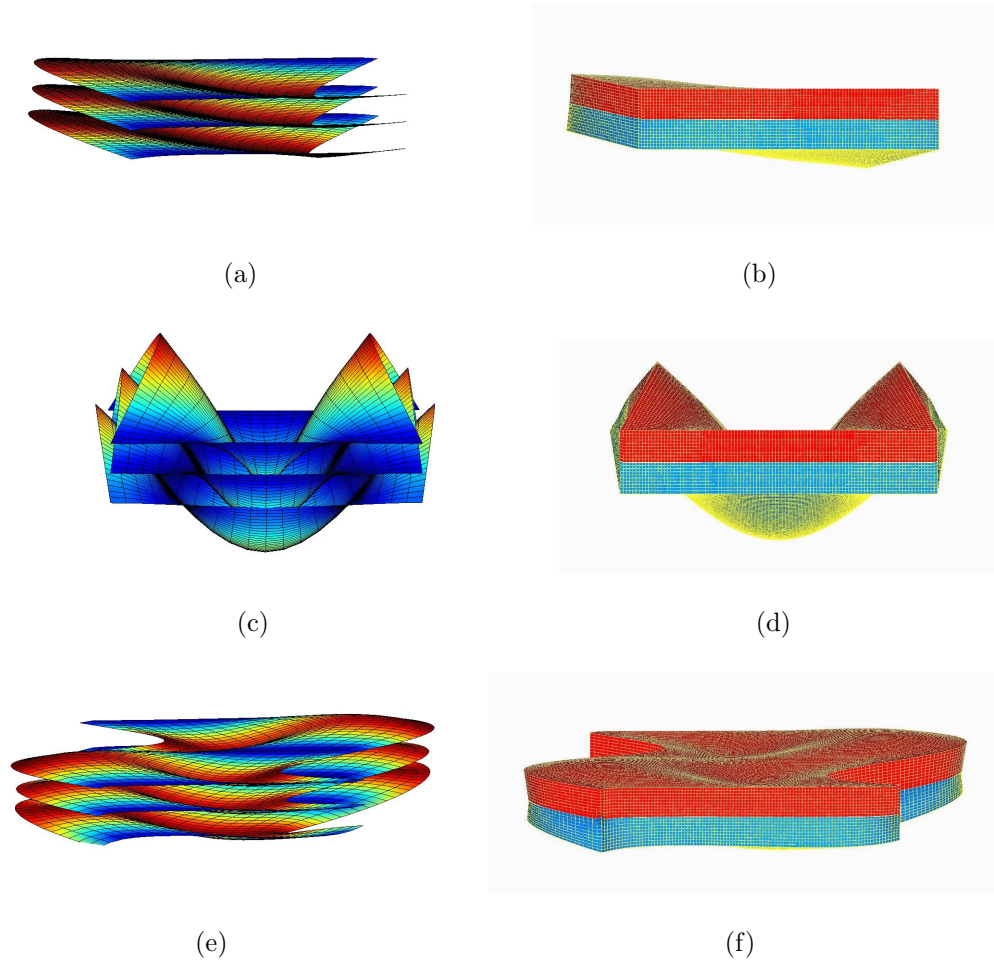


Figure 9: Comparison of some representative mode shapes obtained by DySAP or FEM (NASTRAN) for a SFSF plate. (a) DySAP mode 3, (b) FEM mode 3, (c) DySAP mode 5, (d) FEM mode 5, (e) DySAP mode 9, (f) FEM mode 9.

of a layer wise composite element of n layers has been obtained. This new elements have been validated first against results in the literature for simply supported plates and then compared with 3D and 2D finite element models. The superiority of the dynamic stiffness elements in term of accuracy and computational efficiency has been demonstrated. Exact solutions for layer wise formulation for plates with different boundary conditions, rather than simply supported on the four sides, have been presented for the first time in the literature. These solutions can be used as benchmark to assess other approximate solution methods such as the FEM.

The dynamic stiffness element developed can be rotated, offset and assembled to model more complex structures and yet the exactness of the solution can be retained. The theory presented opens the possibility of carrying out high fidelity free vibration and response analysis of complex composite structures.

Acknowledgements

The authors wish to thank the EPSRC (grant ref: EP/I004904/1) which made this work possible. The authors are also grateful to Prof John Wills (Oxford University), Prof John Fitch (Bath University), Dr Stefanos Giannis (MERL Ltd) and Christopher Morton (SAMTECH) for many stimulating discussions.

APPENDIX A. LAMINATE CONSTITUTIVE EQUATIONS

The constitutive equation for an orthotropic material in the global or laminate reference system can be written as

$$\begin{bmatrix} \sigma_1 \\ \sigma_2 \\ \sigma_3 \\ \sigma_4 \\ \sigma_5 \\ \sigma_6 \end{bmatrix}^k = \begin{bmatrix} C_{11} & C_{12} & C_{13} & 0 & 0 & C_{16} \\ C_{12} & C_{22} & C_{23} & 0 & 0 & C_{26} \\ C_{13} & C_{23} & C_{33} & 0 & 0 & C_{36} \\ 0 & 0 & 0 & C_{44} & C_{45} & 0 \\ 0 & 0 & 0 & C_{45} & C_{55} & 0 \\ C_{16} & C_{26} & C_{36} & 0 & 0 & C_{66} \end{bmatrix}^k \begin{bmatrix} \varepsilon_1 \\ \varepsilon_2 \\ \varepsilon_3 \\ \varepsilon_4 \\ \varepsilon_5 \\ \varepsilon_6 \end{bmatrix}^k \quad (\text{A.1})$$

where

$$\begin{aligned} C_{11} &= \tilde{C}_{11} c^4 + 2(\tilde{C}_{12} + 2\tilde{C}_{66}) c^2 s^2 + \tilde{C}_{22} s^4, \\ C_{12} &= (\tilde{C}_{11} + \tilde{C}_{22} - 4\tilde{C}_{66}) c^2 s^2 + \tilde{C}_{12} (c^4 + s^4) \\ C_{13} &= \tilde{C}_{13} c^2 + \tilde{C}_{23} s^2, \quad C_{16} = -\tilde{C}_{22} c s^3 + \tilde{C}_{11} c^3 s - (\tilde{C}_{12} + 2\tilde{C}_{66}) c s (c^2 - s^2) \\ C_{22} &= \tilde{C}_{11} s^4 + 2(\tilde{C}_{12} + 2\tilde{C}_{66}) c^2 s^2 + \tilde{C}_{22} c^4, \quad C_{23} = \tilde{C}_{13} s^2 + \tilde{C}_{23} c^2 \\ C_{33} &= \tilde{C}_{33}, \quad C_{26} = -\tilde{C}_{22} c^3 s + \tilde{C}_{11} c s^3 + (\tilde{C}_{12} + 2\tilde{C}_{66}) c s (c^2 - s^2) \\ C_{36} &= (\tilde{C}_{13} - \tilde{C}_{23}) c s, \quad C_{44} = \tilde{C}_{44} c^2 + \tilde{C}_{55} s^2 \\ C_{45} &= (\tilde{C}_{55} - \tilde{C}_{44}) c s, \quad C_{55} = \tilde{C}_{55} c^2 + \tilde{C}_{44} s^2 \\ C_{66} &= (\tilde{C}_{11} + \tilde{C}_{22} - 2\tilde{C}_{12}) c^2 s^2 + \tilde{C}_{66} (c^2 - s^2)^2 \end{aligned} \quad (\text{A.2})$$

c and s are

$$c = \cos(\Psi) \quad s = \sin(\Psi) \quad (\text{A.3})$$

where Ψ is the angle from the global or laminate reference system to the lamina or local reference system with coincide with the fibre direction.

The \tilde{C} are the material coefficients in the lamina reference system that can be written as

$$\begin{aligned} \tilde{C}_{11} &= Y_{11} \frac{(1 - \nu_{23}\nu_{32})}{\Delta} , \quad \tilde{C}_{22} = Y_{22} \frac{(1 - \nu_{31}\nu_{13})}{\Delta} , \quad \tilde{C}_{33} = Y_{33} \frac{(1 - \nu_{12}\nu_{21})}{\Delta} \\ \tilde{C}_{44} &= G_{23} , \quad \tilde{C}_{55} = G_{13} , \quad \tilde{C}_{66} = G_{12} \\ \tilde{C}_{12} &= Y_{11} \frac{(\nu_{21} + \nu_{31}\nu_{23})}{\Delta} , \quad \tilde{C}_{13} = Y_{22} \frac{(\nu_{13} + \nu_{12}\nu_{23})}{\Delta} , \quad \tilde{C}_{23} = Y_{33} \frac{(\nu_{23} + \nu_{21}\nu_{13})}{\Delta} \end{aligned} \quad (\text{A.4})$$

where $\Delta = 1 - \nu_{12}\nu_{21} - \nu_{23}\nu_{32} - \nu_{31}\nu_{13} - 2\nu_{21}\nu_{32}\nu_{13}$ and remembering also:

$$\frac{\nu_{ij}}{Y_{ii}} = \frac{\nu_{ji}}{Y_{jj}} \quad (i, j = 1, 2, 3) \quad (\text{A.5})$$

and Y is the elastic modulus, G the shear modulus, ν the poisson ratio, direction 1 the direction of the fibre, 2 the direction perpendicular to the fibre in the plate plane, 3 the out of plane direction perpendicular to the previous two.

APPENDIX B. SOLUTION OF A SYSTEM OF DIFFERENTIAL EQUATION OF THE SECOND ORDER

A system of differential equations of the second order in x can be written as

$$\frac{d^2 \mathbf{y}(x)}{dx^2} = \ddot{\mathbf{y}}(x) = f(\mathbf{y}(x), \dot{\mathbf{y}}(x)) \quad (\text{B.1})$$

where $\mathbf{y}(x) = [y_1, y_2, \dots, y_n]^T$ are the n unknown functions. This can be written in matrix form as

$$\ddot{\mathbf{y}}(x) = \tilde{\mathbf{S}}[\mathbf{y}(x), \dot{\mathbf{y}}(x)]^T \quad (\text{B.2})$$

where \mathbf{S} is the matrix of coefficient whose dimension is $n \times 2n$ and can be written as:

$$\tilde{\mathbf{S}} = \begin{bmatrix} S_{11} & S_{12} & S_{13} & S_{14} & \dots & S_{1(2n-1)} & S_{1(2n)} \\ S_{21} & S_{22} & S_{23} & S_{24} & \dots & S_{2(2n-1)} & S_{2(2n)} \\ \vdots & \vdots & \dots & \dots & \ddots & \vdots & \vdots \\ S_{n1} & S_{n2} & S_{n3} & S_{n4} & \dots & S_{n(2n-1)} & S_{n(2n)} \end{bmatrix} \quad (\text{B.3})$$

By a simple change of variables, the system of second order differential equations can be transformed to a system of first order differential equations. The change of variables is

$$\begin{aligned}
Z_1(x) &= y_1(x), & Z_2(x) &= \dot{y}_1(x) \\
Z_3(x) &= y_2(x), & Z_4(x) &= \dot{y}_2(x) \\
&\vdots \\
Z_{(2n-1)}(x) &= y_n(x), & Z_{(2n)}(x) &= \dot{y}_n(x)
\end{aligned} \tag{B.4}$$

By doing this, a number of first order differential equations will be added to the system in Eq (B.1), such as $\dot{Z}_1 = Z_2$, $\dot{Z}_3 = Z_4$ and $Z_{n-1} = Z_n$, in addition to the original equations in (B.2) which will now be all first order.

If it is linear and the coefficients are constant it can be re-written in matrix form as

$$\dot{\mathbf{Z}}(x) = \mathbf{S}\mathbf{Z}(x) \tag{B.5}$$

where the unknown functions are now:

$$\mathbf{Z}^T = [Z_1, Z_2, Z_3, z_4 \dots, Z_{2n-1}, Z_{2n}] = [y_1, \dot{y}_1, y_2, \dot{y}_2, \dots, y_n, \dot{y}_n] \tag{B.6}$$

and the new matrix of coefficients \mathbf{S} , whose dimension now is $2n \times 2n$ can be written as:

$$\mathbf{S} = \begin{bmatrix}
0 & 1 & 0 & 0 & \dots & 0 & 0 \\
S_{11} & S_{12} & S_{13} & S_{14} & \dots & S_{1(2n-1)} & S_{1(2n)} \\
0 & 0 & 0 & 1 & \dots & 0 & 0 \\
S_{21} & S_{22} & S_{23} & S_{24} & \dots & S_{2(2n-1)} & S_{2(2n)} \\
\vdots & \vdots & \dots & \dots & \ddots & \vdots & \vdots \\
0 & 0 & 0 & 0 & \dots & 0 & 1 \\
S_{n1} & S_{n2} & S_{n3} & S_{n4} & \dots & S_{n(2n-1)} & S_{n(2n)}
\end{bmatrix} \tag{B.7}$$

The solution of first order differential equations in (B.5) can be written as

$$Z_i = \sum_{j=1}^{2n} C_j \delta_{ji} e^{\lambda_j x} \quad (\text{B.8})$$

where C_j are the constant of integration, λ_j is the j^{th} eigenvalue of the matrix \mathbf{S} and δ_{ji} is i^{th} value in the j^{th} eigenvector of the matrix \mathbf{S} . For the sake of simplicity, the solution for Z_1 , i.e. y_1 (see Eq (B.4)) is given in explicit form

$$y_1(x) = C_1 \delta_{11} e^{\lambda_1 x} + C_2 \delta_{21} e^{\lambda_2 x} + \dots + C_{2n} \delta_{(2n)1} e^{\lambda_{2n} x} \quad (\text{B.9})$$

if the eigenvectors are written as a matrix $\boldsymbol{\delta}$ in the following form:

$$\boldsymbol{\delta} = \begin{bmatrix} \delta_{11} & \delta_{21} & \dots & \delta_{(2n)1} \\ \delta_{12} & \delta_{22} & \dots & \delta_{(2n)2} \\ \vdots & \vdots & \ddots & \vdots \\ \delta_{1(2n)} & \delta_{2(2n)} & \dots & \delta_{(2n)(2n)} \end{bmatrix} \quad (\text{B.10})$$

where for δ_{ji} j is the eigenvector number and i is the position in the eigenvector, and the eigenvalues with the constants in the following form:

$$\mathbf{C} e^{\boldsymbol{\lambda} x} = [C_1 e^{\lambda_1 x}, C_2 e^{\lambda_2 x}, \dots, C_{2n} e^{\lambda_{2n} x}]^T \quad (\text{B.11})$$

then the solution in Eq. (B.8) can be written in a more compact matrix form as

$$\mathbf{Z} = \boldsymbol{\delta} \mathbf{C} e^{\boldsymbol{\lambda} x} \quad (\text{B.12})$$

APPENDIX C. FORWARD AND BACKWARD PARTIAL GAUSS ELIMINATION (FBPGE)

The coefficients of the second derivatives are located in the columns which are multiple of 3. In order to decouple the equations, the first row should have -1 in the third column and zero below it, the second row should have -1 in the sixth

column and zeros above and below that and so on. This matrix has been called $\hat{\mathbf{L}}$.

Let us examine a 3 by 9 \mathbf{L} matrix which is fully populated. The algorithm can easily be extended to a matrix of N by N times 3 dimension. The matrix $\hat{\mathbf{L}}$ and subsequently the matrix $\tilde{\mathbf{S}}$ (see Eq. (B.3)) can be obtained by following four steps.

$$\mathbf{L} = \begin{bmatrix} l_{11} & l_{12} & l_{13} & l_{14} & l_{15} & l_{16} & l_{17} & l_{18} & l_{19} \\ l_{21} & l_{22} & l_{23} & l_{24} & l_{25} & l_{26} & l_{27} & l_{28} & l_{29} \\ l_{31} & l_{32} & l_{33} & l_{34} & l_{35} & l_{36} & l_{37} & l_{38} & l_{39} \end{bmatrix} \quad (\text{C.1})$$

- (i) Forward Gauss elimination. Gauss elimination is carried out on entries below l_{13}, l_{26} . This is achieved by the following algorithm for the third column

$$\begin{aligned} l_{2i} &= l_{2i} - \frac{l_{23}}{l_{13}} l_{1i} & \text{for } i = 1, \dots, 9 \\ l_{3i} &= l_{3i} - \frac{l_{33}}{l_{13}} l_{1i} & \text{for } i = 1, \dots, 9 \end{aligned} \quad (\text{C.2})$$

and for the sixth column²

$$l_{3i} = l_{3i} - \frac{l_{36}}{l_{26}} l_{2i} \quad \text{for } i = 1, \dots, 9 \quad (\text{C.3})$$

note that the name of the new element has not been changed for sake of brevity.

The results would be a new \mathbf{L} matrix in the following form

$$\mathbf{L} = \begin{bmatrix} l_{11} & l_{12} & l_{13} & l_{14} & l_{15} & l_{16} & l_{17} & l_{18} & l_{19} \\ l_{21} & l_{22} & 0 & l_{24} & l_{25} & l_{26} & l_{27} & l_{28} & l_{29} \\ l_{31} & l_{32} & 0 & l_{34} & l_{35} & 0 & l_{37} & l_{38} & l_{39} \end{bmatrix} \quad (\text{C.4})$$

- (ii) Backward Gauss Elimination. As before but starting from the third row, ninth column and eliminating everything that is above that element in order

²this algorithm can be generalised for any matrix dimension in a couple of lines

to obtain the following new \mathbf{L} matrix

$$\mathbf{L} = \begin{bmatrix} l_{11} & l_{12} & l_{13} & l_{14} & l_{15} & 0 & l_{17} & l_{18} & 0 \\ l_{21} & l_{22} & 0 & l_{24} & l_{25} & l_{26} & l_{27} & l_{28} & 0 \\ l_{31} & l_{32} & 0 & l_{34} & l_{35} & 0 & l_{37} & l_{38} & l_{39} \end{bmatrix} \quad (\text{C.5})$$

- (iii) Factorisation. It is required to have -1 on the coefficient corresponding to the second derivative so to imply that if that coefficient were to be moved on the other side of the differential equation, its value would be 1. In order to do that the first row is divided by $-l_{13}$, the second by $-l_{26}$ and the third by $-l_{39}$. in this way, the matrix $\hat{\mathbf{L}}$ can be obtained and it has the following form

$$\hat{\mathbf{L}} = \begin{bmatrix} l_{11} & l_{12} & -1 & l_{14} & l_{15} & 0 & l_{17} & l_{18} & 0 \\ l_{21} & l_{22} & 0 & l_{24} & l_{25} & -1 & l_{27} & l_{28} & 0 \\ l_{31} & l_{32} & 0 & l_{34} & l_{35} & 0 & l_{37} & l_{38} & -1 \end{bmatrix} \quad (\text{C.6})$$

- (iii) Eliminate the columns. By eliminating the columns corresponding to the position 3 and it multiples, is equal to move the term containing the second derivatives on the other side of the equations and give the matrix of coefficients associated to the second order differential equation. This matrix has been called $\tilde{\mathbf{S}}$ (see Eq. (B.3)) and following the notation in Eq. (C.6) can be written as

$$\tilde{\mathbf{S}} = \begin{bmatrix} l_{11} & l_{12} & l_{14} & l_{15} & l_{17} & l_{18} \\ l_{21} & l_{22} & l_{24} & l_{25} & l_{27} & l_{28} \\ l_{31} & l_{32} & l_{34} & l_{35} & l_{37} & l_{38} \end{bmatrix} \quad (\text{C.7})$$

List of Figures

1	Example of real stress and displacement fields for multilayered structures [5]	4
2	Example of first order ESL, Zig-Zag and LW displacement distributions through the thickness	5
3	Coordinate system and notations for displacements and forces for a multilayered plate.	21
4	Schematic of how to assemble the \mathbf{L} matrices for each layer to obtain the global \mathbf{L} , i.e. the global system of differential equations	25
5	Schematic of how to assemble the \mathbf{B} matrices for each layer to obtain the global \mathbf{B} , i.e. the global equations of the boundary conditions	27
6	Edge conditions of the plate element and sign conventions	35
7	Assembly of dynamic stiffness matrices	36
8	Comparison of some representative mode shapes obtained by DySAP or FEM (NASTRAN) for a SSSS plate. (a) DySAP mode 1, (b) FEM mode 1, (c) DySAP mode 2, (d) FEM mode 2, (e) DySAP mode 4, (f) FEM mode 4, (g) DySAP mode 6, (h) FEM mode 6.	50
9	Comparison of some representative mode shapes obtained by DySAP or FEM (NASTRAN) for a SFSF plate. (a) DySAP mode 3, (b) FEM mode 3, (c) DySAP mode 5, (d) FEM mode 5, (e) DySAP mode 9, (f) FEM mode 9.	55

References

- [1] R. M. Jones, *Mechanics of Composite Materials*, Mc Graw-Hill, 1975.
- [2] E. Reissner, On the theory of bending of elastic plates, *Journal of Mathematical Physics* 23 (4) (1944) 184–191.
- [3] R. D. Mindlin, Influence of rotatory inertia and shear on flexural vibrations of isotropic, elastic plates, *Journal of Applied Mechanics* 18 (1951) 1031–1036.
- [4] J. N. Reddy, N. D. Phan, Stability and vibration of isotropic, orthotropic and laminated plates according to a higher-order shear deformation theory, *Journal of Sound and Vibrations* 98 (2) (1985) 157–170.
- [5] E. Carrera, c_z^0 requirements - models for the two dimensional analysis of multilayered structures, *Composite Structures* 37 (3-4) (1997) 373–383.
- [6] N. J. Pagano, Exact solution for bidirectional composites and sandwich plates, *Journal of Composite Materials* 4 (20-36).
- [7] H. Murakami, Laminated composite plate theory with improved in-plane responses., *Journal of Applied Mechanics, Transactions ASME* 53 (3) (1986) 661–666.
- [8] A. Tessler, M. Di Sciuva, M. Gherlone, Refined zigzag theory for laminated composite and sandwich plates, Tech. Rep. TP-2009-215561, NASA, Lagley, Virginia (2009).
- [9] A. Tessler, M. Di Sciuva, M. Gherlone, A consistent refinement of first-order shear deformation theory for laminated composite and sandwich plates using improved zigzag kinematics, *Journal of Mechanics of Materials and Structures* 5 (2) (2010) 341–367.

- [10] E. Cosentino, P. Weaver, An enhanced single-layer variational formulation for the effect of transverse shear on laminated orthotropic plates, *European Journal of Mechanics, A/Solids* 29 (4) (2010) 567–590.
- [11] E. Srinivas, A refined analysis of composite laminates, *Journal of Sound and Vibration* 30 (1973) 495–507.
- [12] E. Carrera, M. Boscolo, Classical and mixed finite elements for static and dynamic analysis of piezoelectric plates, *International journal for numerical methods in engineering* 70 (2007) 1135–1181.
- [13] E. Carrera, Mixed layer-wise models for multilayered plates analysis, *Composite Structures* 43 (1) (1998) 57–70.
- [14] E. Carrera, L. Demasi, Classical and advanced multilayered plate elements based upon pvd and rmvt. part 1: Derivation of finite element matrices, *International Journal for Numerical Methods in Engineering* 55 (2) (2002) 191–231.
- [15] E. Carrera, L. Demasi, Classical and advanced multilayered plate elements based upon pvd and rmvt. Part 2: Numerical implementations, *International Journal for Numerical Methods in Engineering* 55 (3) (2002) 253–291.
- [16] E. Carrera, M. Boscolo, A. Robaldo, Hierarchic multilayered plate elements for coupled multifield problems of piezoelectric adaptive structures: Formulation and numerical assessment, *Archives of computational methods in engineering* 14 (2007) 383–430.
- [17] E. Carrera, S. Brischetto, A survey with numerical assessment of classical and refined theories for the analysis of sandwich plates, *ASME Applied Mechanics Reviews* 62 (1) (2009) 1–17.

- [18] E. Carrera, Layer-wise mixed models for accurate vibration analysis of multilayered plates, *ASME* 65 (4) (1998) 820–828.
- [19] E. Carrera, A study of transverse normal stress effect on vibration of multilayered plates and shells, *Journal of Sound and Vibrations* 225 (5) (1999) 803–829.
- [20] E. Carrera, L. Demasi, M. Manganello, Assessment of plate elements on bending and vibrations of composite structures, *Mechanics of Advanced Materials and Structures* 9 (2002) 333–357.
- [21] O. C. Zienkiewicz, R. L. Taylor, *The Finite element method*, 5th Edition, Vol. 1: The basis, Butterworth-Heinemann, 2000.
- [22] E. Carrera, Theories and finite elements for multilayered plates and shells: A unified compact formulation with numerical assessment and benchmarking, *Archives of Computational Methods in Engineering* 10 (3) (2003) 1–81.
- [23] E. Carrera, Theories and finite elements for multilayered, anisotropic, composite plates and shells, *Archives of Computational Methods in Engineering* 9 (2) (2002) 87–140.
- [24] J. R. Banerjee, Dynamic stiffness formulation for structural elements: A general approach, *Computers and Structures* 63 (1) (1997) 101–103.
- [25] J. R. Banerjee, Coupled bending-torsional dynamic stiffness matrix for beam elements, *International Journal of Numerical Methods in Engineering* 28 (1989) 1283–1298.
- [26] J. R. Banerjee, Free vibration analysis of a twisted beam using the dynamic stiffness method, *International Journal of Solids and Structures* 38 (38-39) (2001) 6703–6722.

- [27] J. R. Banerjee, Free vibration of sandwich beams using the dynamic stiffness method, *Computers and Structures* 81 (18-19) (2003) 1915–1922.
- [28] J. R. Banerjee, Development of an exact dynamic stiffness matrix for free vibration analysis of a twisted timoshenko beam, *Journal of Sound and Vibration* 270 (1-2) (2004) 379–401.
- [29] J. R. Banerjee, H. Su, D. R. Jackson, Free vibration of rotating tapered beams using the dynamic stiffness method, *Journal of Sound and Vibration* 298 (4-5) (2006) 1034–1054.
- [30] J. R. Banerjee, C. W. Cheung, R. Morishima, M. Perera, J. Njuguna, Free vibration of a three-layered sandwich beam using the dynamic stiffness method and experiment, *International Journal of Solids and Structures* 44 (22-23) (2007) 7543–7563.
- [31] F. W. Williams, W. H. Wittrick, An automatic computational procedure for calculating natural frequencies of skeletal structures, *International Journal of Mechanical Sciences* 12 (9) (1970) 781–791.
- [32] W. H. Wittrick, A unified approach to initial buckling of stiffened panels in compression, *International Journal of Numerical Methods in Engineering* 11 (1968) 1067–1081.
- [33] W. H. Wittrick, General sinusoidal stiffness matrices for buckling and vibration analyses of thin flat-walled structures, *International Journal of Mechanical Sciences* 10 (1968) 949–966.
- [34] F. W. Williams, W. H. Wittrick, Computational procedures for a matrix analysis of the stability and vibration of thin flat-walled structures in compression, *International Journal of Mechanical Sciences* 11 (12) (1969) 979–998.

- [35] W. H. Wittrick, F. W. Williams, Buckling and vibration of anisotropic or isotropic plate assemblies under combined loadings, *International Journal of Mechanical Sciences* 16 (4) (1974) 209–239.
- [36] W. Anderson, J. Stroud, B. J. Durling, K. W. Hennessy, Structural panel analysis and sizing code, Tech. Rep. TM-80182, NASA, Lagley, Virginia (November 1981).
- [37] J. Stroud, W. H. Greene, W. Anderson, Buckling loads for stiffened panels subjected to combined longitudinal compression and shear loading, Tech. Rep. TM-83194, NASA, Lagley, Virginia (October 1981).
- [38] M. Anderson, F. Williams, C. Wright, Buckling and vibration of any prismatic assembly of shear and compression loaded anisotropic plates with an arbitrary supporting structure, *International Journal of Mechanical Sciences* 25 (8) (1983) 585–596.
- [39] F. Williams, J. Banerjee, Accurately computed modal densities for panels and cylinders, including corrugations and stiffeners, *Journal of Sound and Vibration* 93 (4) (1984) 481–488.
- [40] F. W. Williams, D. Kennedy, R. Butler, M. S. Anderson, VICONOPT: Program for exact vibration and buckling analysis or design of prismatic plate assemblies, *AIAA Journal* 29 (1991) 1927–1928.
- [41] M. Anderson, D. Kennedy, Transverse shear deformation in the exact buckling and vibration analysis of composite plate assemblies, *AIAA Journal* 31 (10) (1993) 1963–1965.

- [42] M. Anderson, D. Kennedy, Inclusion of transverse shear deformation in the exact buckling and vibration analysis of composite plate assemblies, Tech. Rep. Contractor report 4510, NASA, Lagley, Virginia (1993).
- [43] M. Boscolo, J. R. Banerjee, Dynamic stiffness elements and their applications for plates using first order shear deformation theory, *Computers and Structures* 89 (2010) 395–410.
- [44] M. Boscolo, J. R. Banerjee, Dynamic stiffness method for exact inplane free vibration analysis of plates and plate assemblies, *Journal of Sound and Vibration* 330 (2011) 29282936.
- [45] M. Boscolo, R. J. Banerjee, Dynamic stiffness formulation for composite mindlin plates for exact modal analysis of structures. Part I: Theory, *Computers and Structures* 96–97 (2012) 61–73.
- [46] M. Boscolo, R. J. Banerjee, Dynamic stiffness formulation for composite mindlin plates for exact modal analysis of structures. Part II: Results and applications, *Computers and Structures* 96–97 (2012) 73–84.
- [47] M. S. Anderson, F. W. Williams, BUINVIS-RG: Exact frame buckling and vibration program, with repetitive geometry and substructuring., *Journal of spacecraft rockets* 24 (1987) 353–361.
- [48] B. Akkeson, A computer program for plane frame vibration analysis by an exact method, *International Journal of numerical methods in engineering* 10 (1976) 1221–1231.
- [49] F. Fazzolari, M. Boscolo, J. Banerjee, An exact dynamic stiffness element using a higher order shear deformation theory for free vibration analysis of composite plate assemblies, *Composite Structures* 96 (2013) 262–278.

- [50] M. Boscolo, J. R. Banerjee, Dynamic stiffness laminate elements for exact modal analysis of aeronautical structures, in: 53st AIAA/ASME/ASCE/AHS/ASC Structures, Structural Dynamics, and Materials Conference, Waikiki, Hawaii, USA, 2012.
- [51] E. Carrera, S. Brischetto, Analysis of thickness locking in classical, refined and mixed multilayered plate theories, *Composite Structures* 82 (4) (2008) 549–562.
- [52] A. W. Leissa, *Vibration of plates*, Tech. Rep. NASA SP-160, National Aeronautics and space administration, Washington (1969).
- [53] I. Chopra, Vibration of stepped thickness plates, *International Journal of Mechanical Sciences* 16 (1974) 337–344.
- [54] U. Lee, *Spectral Element Method in Structural Dynamics*, 1st Edition, John Wiley & Sons, 2009.
- [55] W. H. Wittrick, F. W. Williams, A general algorithm for computing natural frequencies of elastic structures, *Quarterly Journal of mechanics and applied sciences* 24 (3) (1970) 263–284.
- [56] A. Noor, B. W.S., Stress and free vibration analyses of multilayered composite plates, *Composite structures* 11 (1989) 183–204.
- [57] E. Carrera, An assessment of mixed and classical theories on global and local response of multilayered orthotropic plates, *Composite Structures* 50 (2000) 183–198.
- [58] L. Dozio, Ritz analysis of vibrating rectangular and skew multilayered plates based on advanced variable-kinematic models, *Composite Structures* 94 (2118-2128).